Supplementary information

Covalent organic frameworks as nanocarriers of tailored BODIPY for phototheragnostic applications

Miguel Jiménez-Duro, Paula M. Soriano-Teruel, Marcos Martínez-Fernández, Edurne Avellanal-Zaballa, Jennifer Soler-Beatty, José I. Martínez, Alba García-Fernández, María J. Ortiz, Gonzalo Durán-Sampedro,* Jorge Bañuelos,* Ramón Martínez-Máñez,* José L. Segura*

Table of contents

Section S1. Experimental section

S1.1. Materials

All commercially available reagents were used as received. TAPB, DMTA and BAETA were synthetized as previously reported.[1]

S1.2. Characterization methods

(^{13}C CP/MAS-NMR) spectra were recorded on a Bruker AVANCE III HD-WB 400 MHz with a rotation frequency of 12 kHz.

Fourier transformed infrared (FT-IR) spectroscopy was performed on a PerkinElmer 100 spectrophotometer equipped with a PIKE Technologies MIRacle Single Reflection Horizontal ATR Accessory and on a Bruker TENSOR 27 on a diamond plate.

Powder x-ray diffraction (PXRD) measurements were carried out with X'PERT MPD with conventional Bragg-Brentano geometry using monochromatic Cu Kα1 radiation (λ = 1.5406 Å) in the 2θ = 2° - 40° range.

N_2 sorption isotherms. N_2 (77 K) adsorption-desorption measurements were carried out on a Micromeritics Tristar 3000. Samples were previously activated for 4 h under high vacuum ($<10^{-7}$ bar) at 120 °C.

Thermogravimetric anlysis (TGA) and differential scanning calorimetry (DSC) measurements were recorded on a Thermobalance TGA 500 (TA Instruments) with a heating ramp from 20 °C to 830 °C at 10 °C min^{-1}, under N_2 atmosphere.

Dynamic light scattering (DLS) measurements were acquired on an ALV CGS-8 multiangle photonic correlation spectrometer.

Scanning Electron Microscopy (SEM) images were acquired on a JEOL JSM 7600F microscope.

Transmission electron microscopy (TEM) micrographs were recorded in a JEOL JEM 1400 TEM at 60 kV.

Computational Methods. As starting point, the theoretical investigation of the molecular fragments involved in the formation of the different **PS1**, **PS2** and **PS3** COF-systems was carried out by density functional theory (DFT) as implemented in the Gaussian 16 C.01 atomistic simulation package.[2]The M062X functional[3] was adopted to account for the exchange-correlation energy, and the cc-pVTZ basis set[4] for the all-electron modelling of all the atoms involved. All geometric parameters were allowed to vary independently, and frequency calculations confirmed the calculated geometries as minima. For the periodic calculations, periodic boundary conditions

were applied for simultaneous structure + cell optimizations of various stacked 3D layered COF model systems based on their canonical 2D network structures. CASTEP plane-wave DFT code[5] was used to construct optimized 2D networks with the GGA-PBE functional[6] accounting for exchange-correlation effects. Tkatchenko-Scheffler van der Waals correction scheme[7] was used to include dispersion forces. Ultra-soft pseudopotentials[8] were adopted to model ion-electron interactions, and Brillouin zones were sampled using [2 × 2 × 1] and [2 × 2 × 8] Monkhorst-Pack grids[9] for 2D layers and 3D crystals, respectively. Full structure + cell optimizations involved atomic relaxations until forces on any atom were below 0.02 eV $Å^{-1}$, including interlayer distances. Several eclipsed (AA) configurations were analyzed for crystal-bulk models (no other topologically consistent). The optical absorption spectra for the periodic systems were computed within the time-dependent density functional theory (TDDFT) framework as implemented in CASTEP. The Tamm-Dancoff approximation (TDA) was employed to simplify the solution of the excited-state response equations by neglecting the coupling between resonant and anti-resonant terms, providing an accurate description of the main photoabsorption features while maintaining computational efficiency.[10]

S.1.3. Photophysical details

The photophysical properties of the dyes (PS1-PS3) in solution were registered using quartz cuvettes of 1 cm path length from diluted solutions (around 2×10^{-6} M), prepared by adding the corresponding solvent to the residue from the adequate amount of a concentrated stock solution in acetone, after vacuum evaporation of this solvent. The photophysical properties of the BODIPY-COF nanoparticles (PS1-, PS2-, PS3-COF) were registered, with the above cuvettes, dispersing 1 mg of the sample in 5 ml of solvent (chloroform) and under vigorous and prolonged stirring. UV-Vis absorption and fluorescence spectra were recorded on a CARY 7000 spectrophotometer (Agilent) and an Edinburgh Instruments spectrofluorometer (model FLSP 920), respectively. The recording of the absorption spectra of the suspensions was done in an integrating sphere, in transmittance mode, to decrease the effect of the light dispersion from the nanoparticles. The baseline was recorded using a suspension of COF without the PS as blank. Fluorescence quantum yields (ϕ_{fl}) were obtained from corrected spectra (detector sensibility to the wavelength) using as references commercial PM546 (ϕ_{fl} = 0.81 in methanol) for PS1, PM597 (ϕ_{fl} = 0.47 in ethyl acetate) for PS2, and cresyl violet (ϕ_{fl} = 0.54 in methanol) for PS3. These values were corrected by the refractive index of the solvent. For the suspensions containing the nanoparticles (PS1-, PS2- and PS3-COF), the absolute fluorescence efficiencies were recorded by means of an integrating sphere coupled to the spectrofluorometer. Radiative decay curves were registered with the time correlated single-photon counting technique as implemented in the aforementioned spectrofluorometer. Fluorescence emission was monitored at the maximum emission wavelengths after excitation by means of a Fianium pulsed laser (time resolution of

picoseconds) with tunable wavelength. The fluorescence lifetime (τ_{fl}) was obtained after the deconvolution of the instrumental response signal from the recorded decay curves by means of an iterative method. The goodness of the exponential fit was controlled by statistical parameters (chi-square, Durbin-Watson and the analysis of the residuals). Nanosecond transient absorption spectra (ns-TAS) were recorded on a LP 980 laser flash photolysis spectrometer (Edinburgh Instruments). Samples were excited by a nanosecond pulsed laser (Nd:YAG laser, LOTIS TII 2134) operating at 1 Hz and a pulse width of ≥ 7 ns, coupled to an OPO which allows the selection of the excitation wavelength. The transient signals were recorded on single detector (PMT R928P), oscilloscope for kinetic traces and ICCD detector DH320T TE cooled (Andor Technology) for time resolved spectra. Samples were measured deaerated with nitrogen for *ca.* 15 min before each measurement.

The photoinduced production of singlet oxygen ($^1O_2$) was determined by direct measurement of the luminescence at 1276 nm with a NIR detector integrated in the aforementioned spectrofluorometer (InGaAs detector, Hamamatsu G8605-23). The $^1O_2$ signal was registered in front configuration (front face), 40° and 50° to the excitation and emission beams, respectively and leaned 30° to the plane formed by the direction of incidence and registration in cells of 1 cm. The signal was filtered by a low cut-off of 850 nm. $^1O_2$-generation quantum yield (ϕ^{Δ}) was determined using the following equation:

$$\phi^{\Delta} = \phi^{\Delta,r} \cdot (\alpha^{r}/\alpha^{PS}) \cdot (Se^{PS}/Se^{r})$$

where $\phi^{\Delta,r}$ is the quantum yield of $^1O_2$ generation for the used reference; 2,6-diiodo-3,5-dimethyl-8-methylthioBODIPY (MeSBDP, being 0.91 in chloroform) for PS2 free and linked to COF, and new methylene blue (being 0.50 in chloroform) for PS3 free an linked to COF. Factor $\alpha = 1\text{-}10^{-Abs}$, corrects the different amount of photons absorbed by the sample (α^{PS}) and reference (α^{R}). Factor Se is the intensity of the $^1O_2$ phosphorescence signal of the sample (Se^{PS}) and the reference (Se^{r}) at 1276 nm. $^1O_2$ quantum yields were averaged from at least five concentrations between 10^{-6} M and 10^{-5} M.

S1.4. Biological studies.

Phototoxicity evaluation in cell culture

The phototoxic capacity of COF nanoparticles, PS1-COF, PS2-COF and PS3-COF was evaluated in SK-Mel-103 cells by using the WST-1 Assay for Cell Proliferation and Viability (Roche, Switzerland). For this, $5x10^3$ cells/well were seeded in a 96-well plate and were kept in the incubator for 24 h prior to treatment. Next, each PS-COFs was then incorporated in the medium at the concentrations indicated in the text and incubated with the cells for 24 h. Afterwards, cells were rinsed with a PBS solution and replaced with fresh medium and irradiated with a 36 W LED

device at 10 cm (900mW/cm^2) of distance during 30 min (i.e., 1620 J/cm2light dose). To allow the passage only of the wavelength capable of exciting the compounds a Longpass Filter Color Red Glass ($\lambda > 610$ nm) or Green Glass ($\lambda > 475$ nm) was incorporated between the light source and the 96-well plate. After irradiating the 96-well plate, the cells were incubated for another 24 h and then 10 µL of WST-1 was added to each well and were further incubated for 2 h at 37 ^{0}C. Finally, the absorbance of the cellular medium was measured at a wavelength of $\lambda = 450$ nm with the spectrophotometer Wallac 1420 Victor2 Microplate Reader (PerkinElmer, USA). The intrinsic toxicity of the compound, without the effect of light exposure, was evaluated under the same conditions but omitting the irradiation treatment step. The IC_{50} which refers to the concentration of compound which reduced 50% of cell viability compared to the untreated controls was calculated from a sigmoidal curve fit of the photocytotoxicity data for at least three independent measurements for the same compound.

Subcellular co-localization studies

To carry out the subcellular co-localization studies, 2.5 x 10^4 SK-Mel-103 cells were seeded on 24 nm φ glass coverslips previously introduced, under sterile conditions, in a 6-well plate and incubated at 37 ^{0}C for 24 h. Then, cells were treated with PS3-COF at a concentration of 10 µg/mL for 24 h. Next, cells were rinsed with 2 mL of PBS saline solution and incubated with different subcellular-specific trackers (Molecular Probes ® by Life Technologies, USA) in green. For specific labeling of lysosomes, cells were incubated with 75 nM Lysotracker green for 2 h and for labeling of lipid droplets (LDs) with 10 µM PM546 (1,3,5,7,8-pentamethylpyrromethene-difluoroborate complex, Luxottica / Exciton, USA) green for 30 min. In addition, the nuclei of the cells were stained by incorporating the fluorescent dye Hoechst 33258 (2 µg/mL) for 15 min prior to visualization in the confocal microscopy Leica (Germany) TCS SP8 HyVolution II. To visualize the nuclei, the Hoechst 33258 was excited with the 405 nm laser and the fluorescence emitted in the range of 415-475 nm was collected. To excite the cellular markers in green, the 488 nm wavelength laser was used, and the fluorescence emitted between 490-530 nm was collected and finally **PS3-COF** was excited with the 532 laser and the emission was collected in the range of 640-780 nm. To analyse the degree of co-localization between the specific subcellular markers and **PS3-COF**, the Person's correlation coefficient (R) was calculated from the images obtained by confocal using the LAS X program. It is considered that there is a co-localization when R values are ≥ 0.7.

ROS production in cells

To evaluate the capacity to generate reactive oxygen species (ROS) of PS3-COF in SK-Mel-103 cell line, the marker CM-H2DCFDA green (General Oxidative Stress Indicator, Invitrogen, ThermoFisher, USA) was used. Firstly, SK-Mel-103 cells were seeded in a density of 25x10^4

cells/well on 24 nm φ glass coverslips previously introduced, under sterile conditions, in a 6-well plate and incubated at 37 ^{0}C for 24 h. Afterwards, 10 μg/mL of PS3-COF was added to the culture medium and left for 24 h, then the cells were rinsed with 2 mL of PBS and places in fresh medium. Then, cells were irradiated following the same protocol used to analyse the phototoxic capacity and the marker CM-H2DCFDA in green was incorporated at a final concentration of 500 nM during 15 min incubation. Confocal images were taken in the confocal microscopy Leica TCS SP8 HyVolution II and mean fluorescence intensity of the probe was obtained with ImageJ/Fiji. CM-H2DCFDA was exited at 488 nm and emission read at 511 ± 23 nm.

Statistical analysis

The *in vitro* experiments using cell lines were performed at least three times independently, with the results shown in the text being representative for each of the studies. Data is presented in the graphs and in the text as mean ± standard deviation of the mean (SEM) obtained by the software GraphPad Prism 8.0. Statistical significance was assessed using the appropriate method according to the data analysing, in this case either the two-tailed Student's t-test or the one-way / two-way ordinary ANOVA was used. It is considered that there is a significant difference between two populations when the p-value < 0.05.

Section S2. Characterization

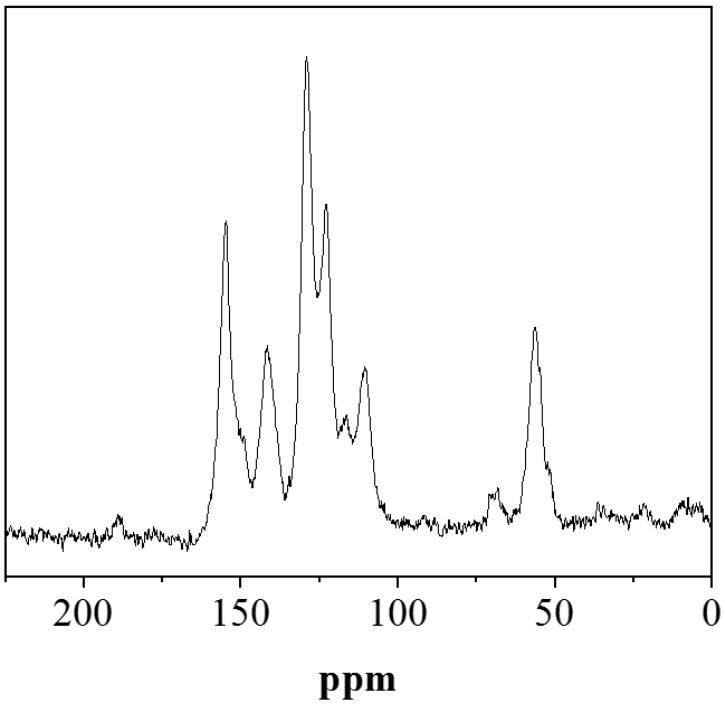

Figure S1. ^{13}C CP/MAS-NMR of COF nanoparticles.

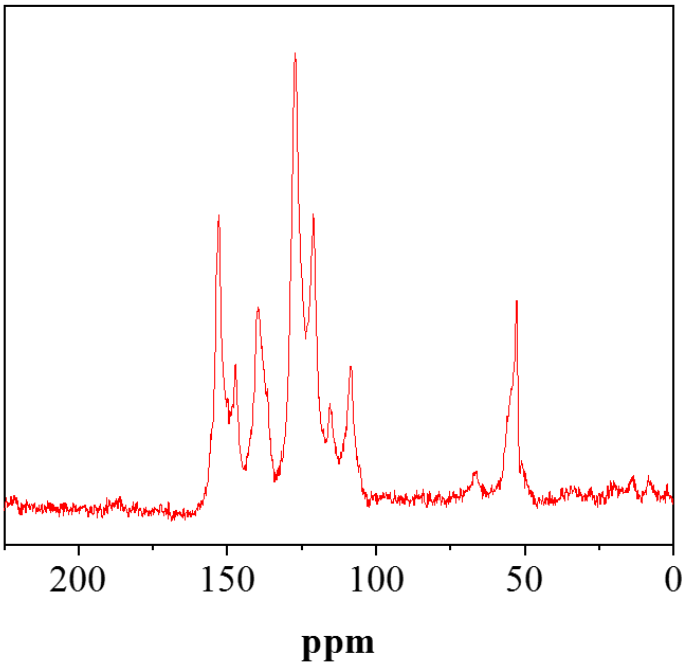

Figure S2. ^{13}C CP/MAS-NMR of PS1-COF.

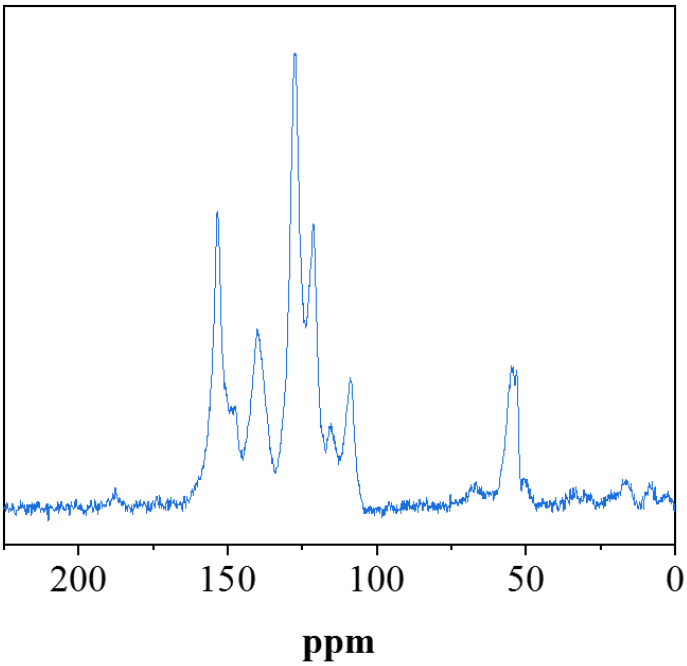

Figure S3. ^{13}C CP/MAS-NMR of PS2-COF.

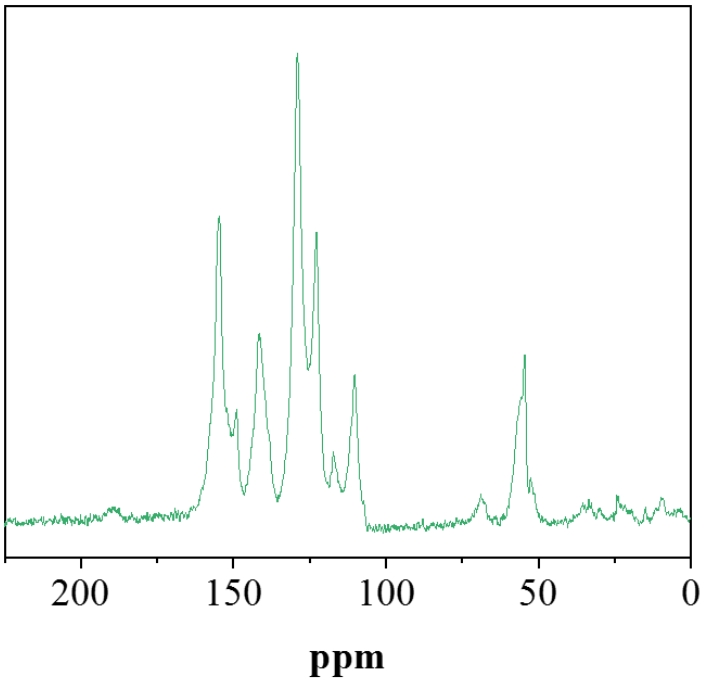

Figure S4. ^{13}C CP/MAS-NMR of PS3-COF.

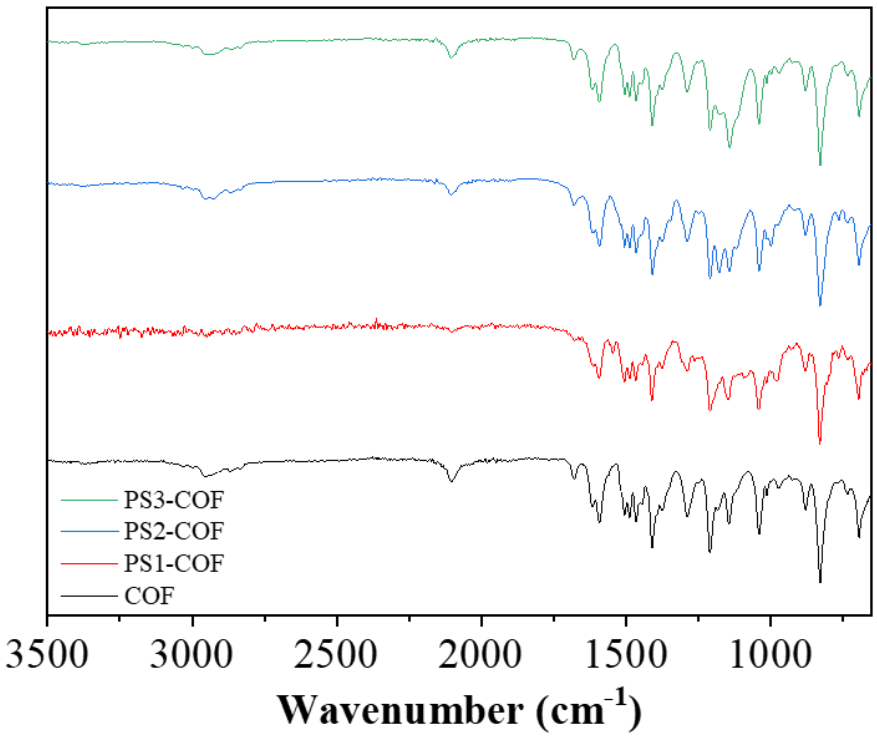

Figure S5. Comparison between the FTIR spectra of COF nanoparticles (black), PS1-COF (red), PS2-COF (blue) and PS3-COF (green).

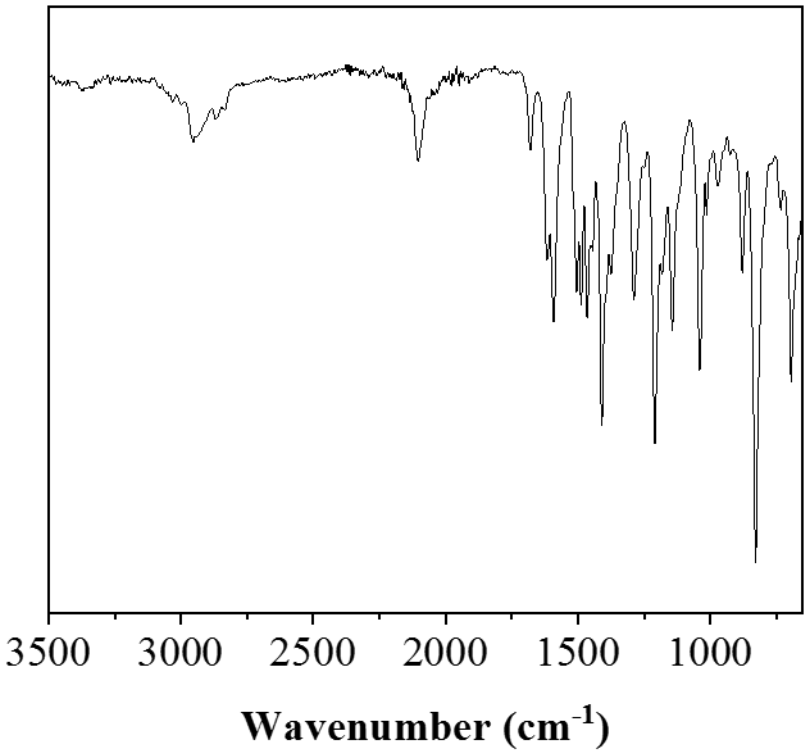

Figure S6. FTIR spectra of COF nanoparticles.

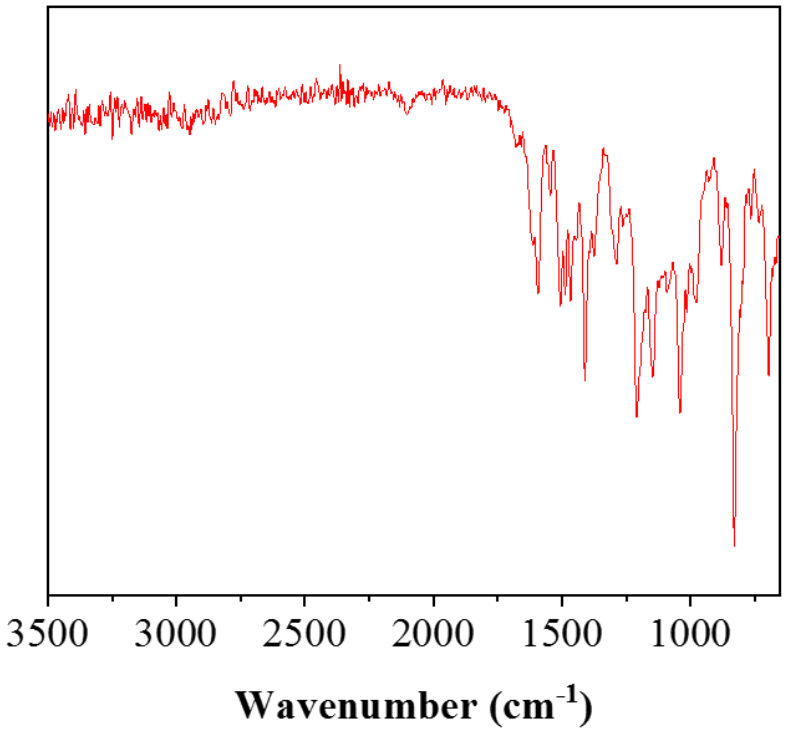

Figure S7. FTIR spectra of PS1-COF.

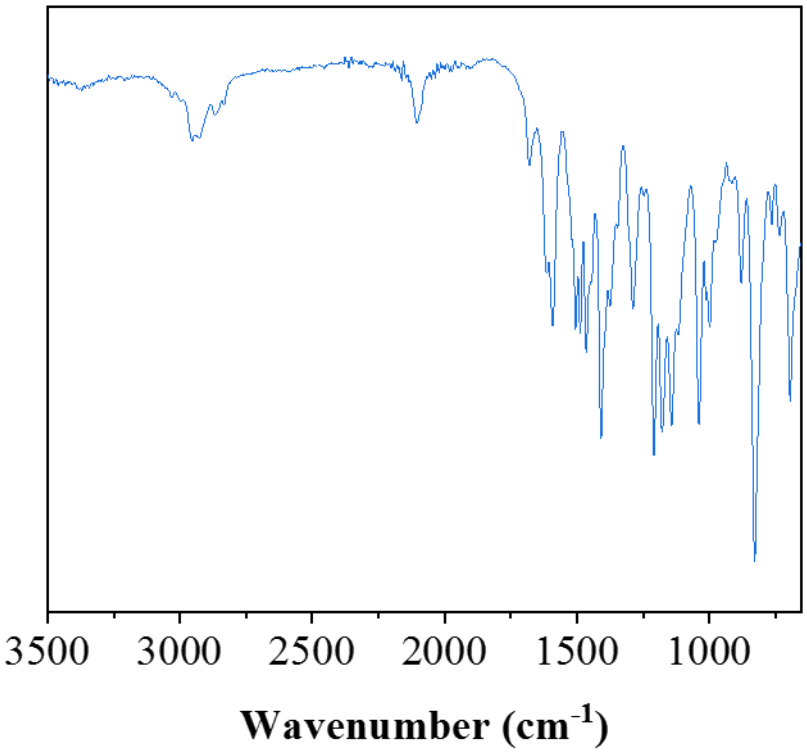

Figure S8. FTIR spectra of PS2-COF.

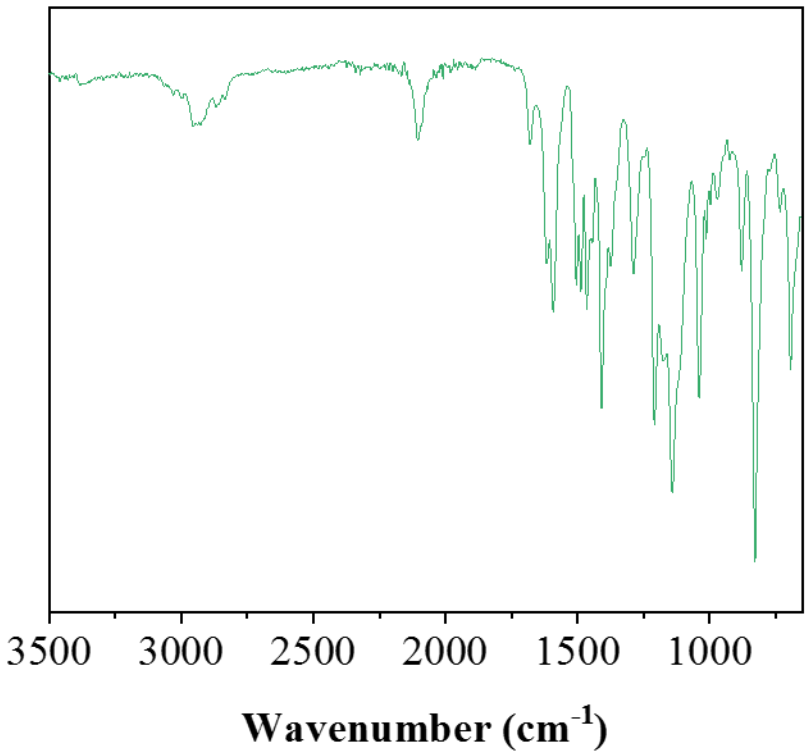

Figure S9. FTIR spectra of PS3-COF.

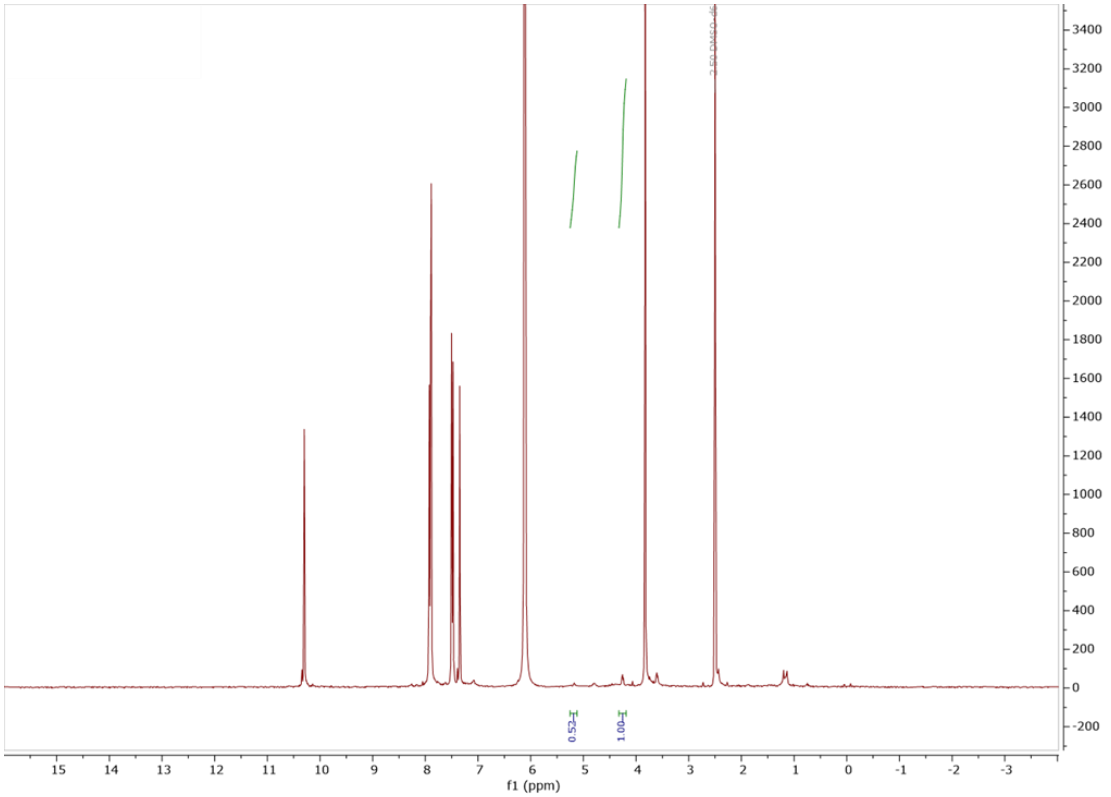

Figure S10. NMR spectra of dissolved PS2-COF.

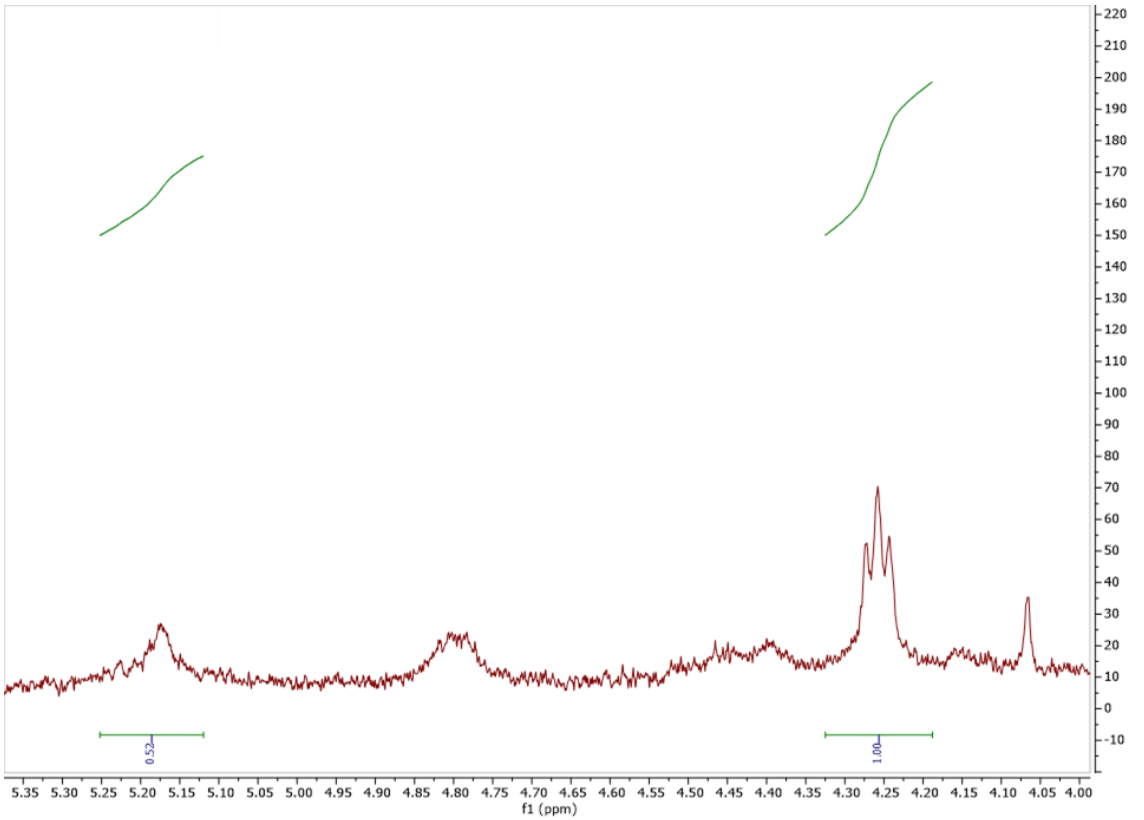

Figure S11. Magnification of the NMR spectra of dissolved PS2-COF of both CH_2 α carbons.

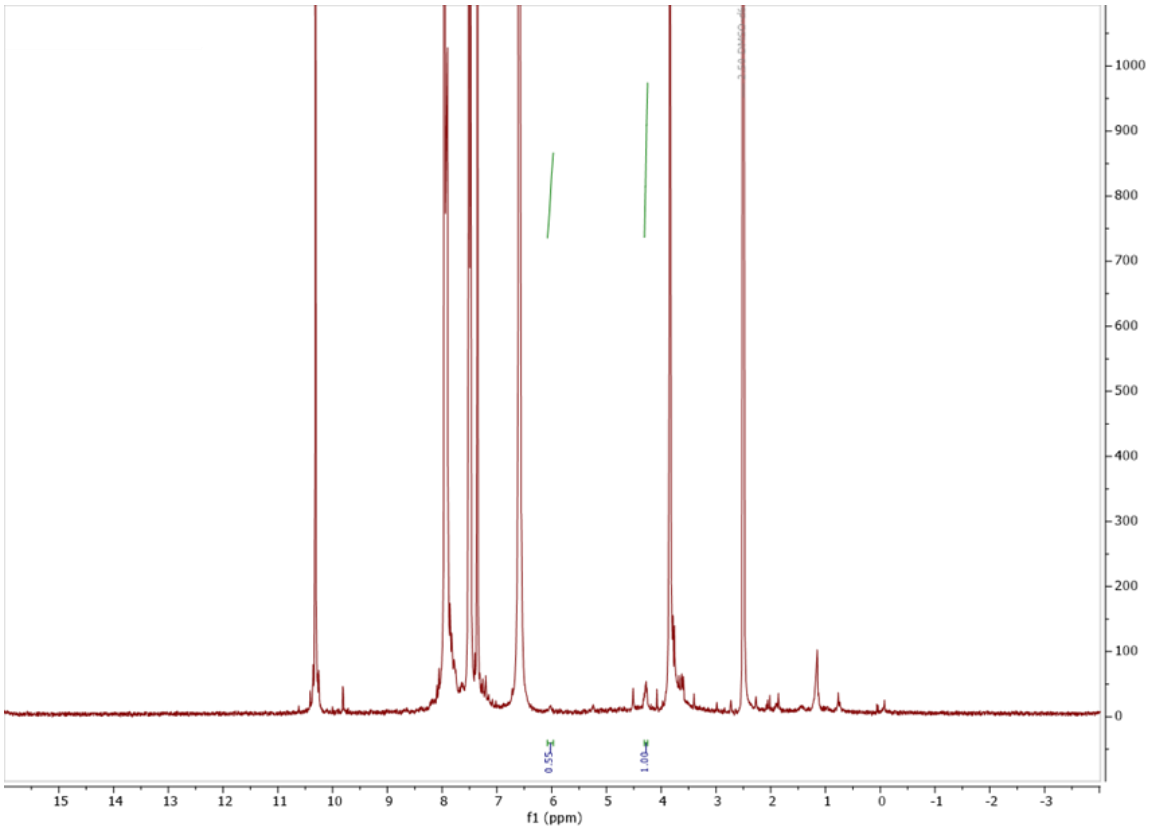

Figure S12. NMR spectra of dissolved PS3-COF.

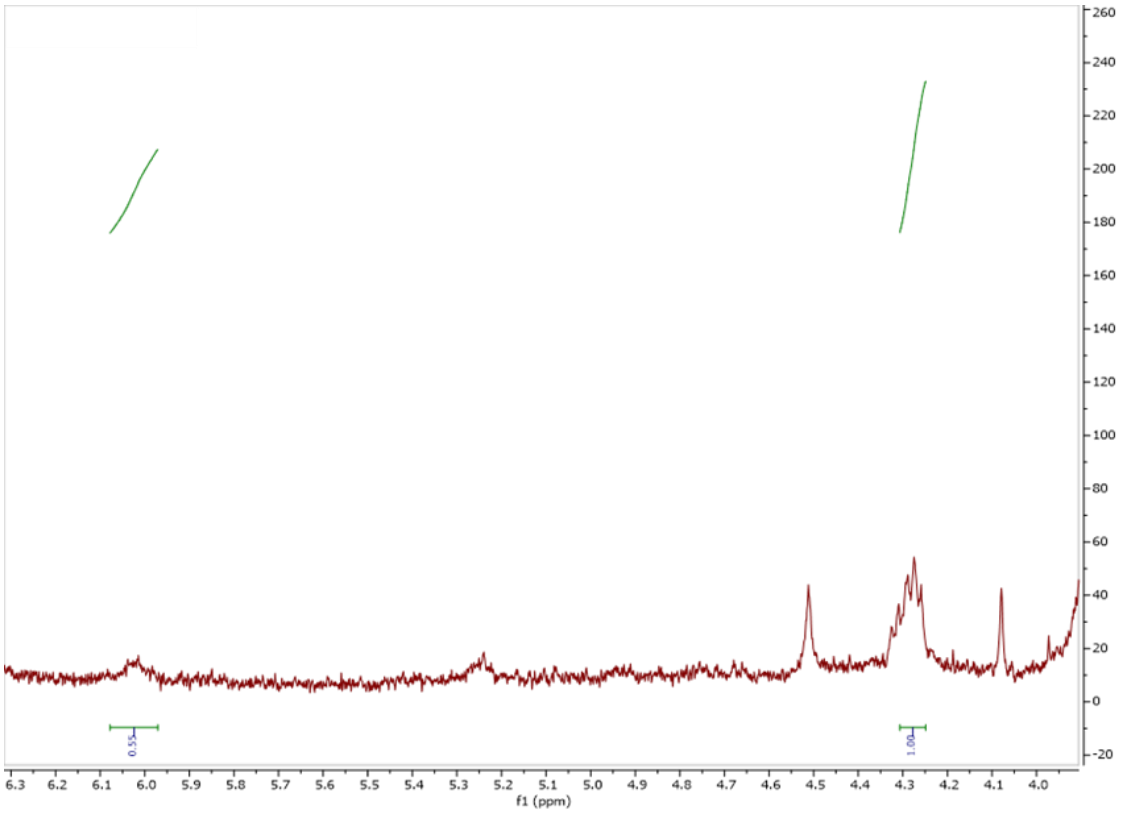

Figure S13. Magnification of the NMR spectra of dissolved PS3-COF of both CH_2 α carbons.

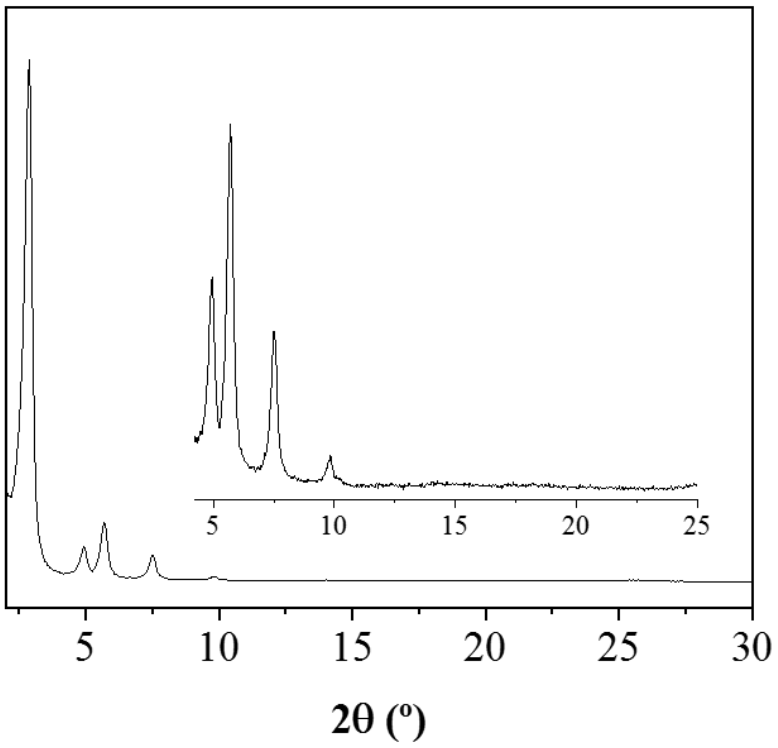

Figure S14. PXRD of COF nanoparticles and a magnification between 4º and 25º.

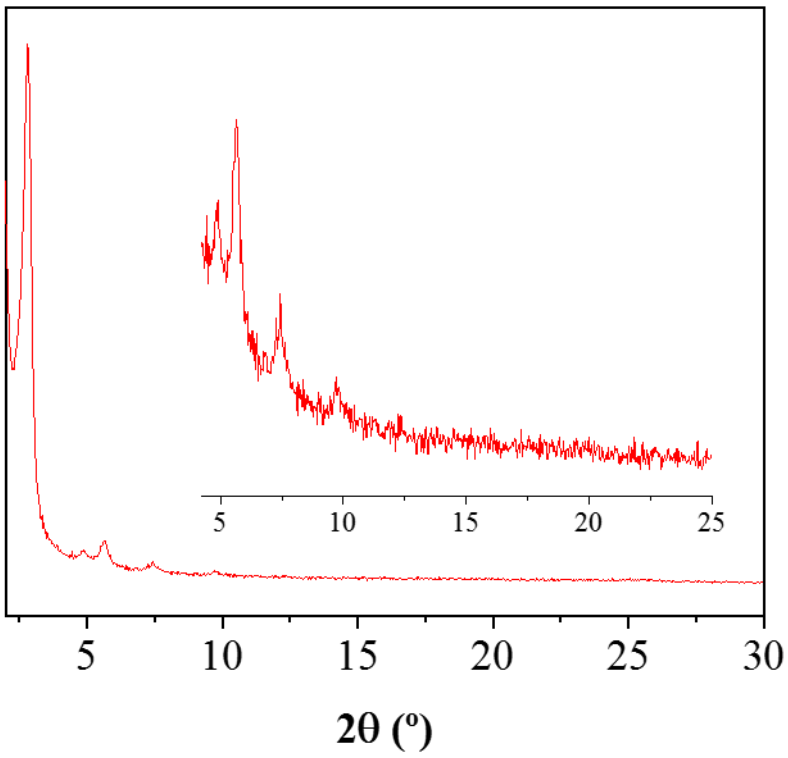

Figure S15. PXRD of PS1-COF and a magnification between 4º and 25º.

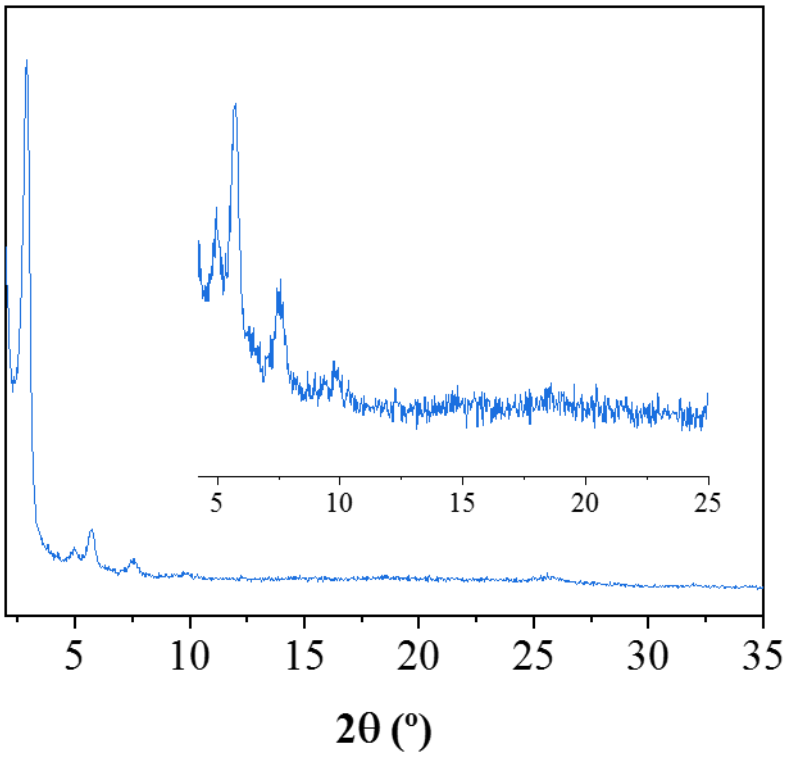

Figure S16. PXRD of PS2-COF and a magnification between 4º and 25º.

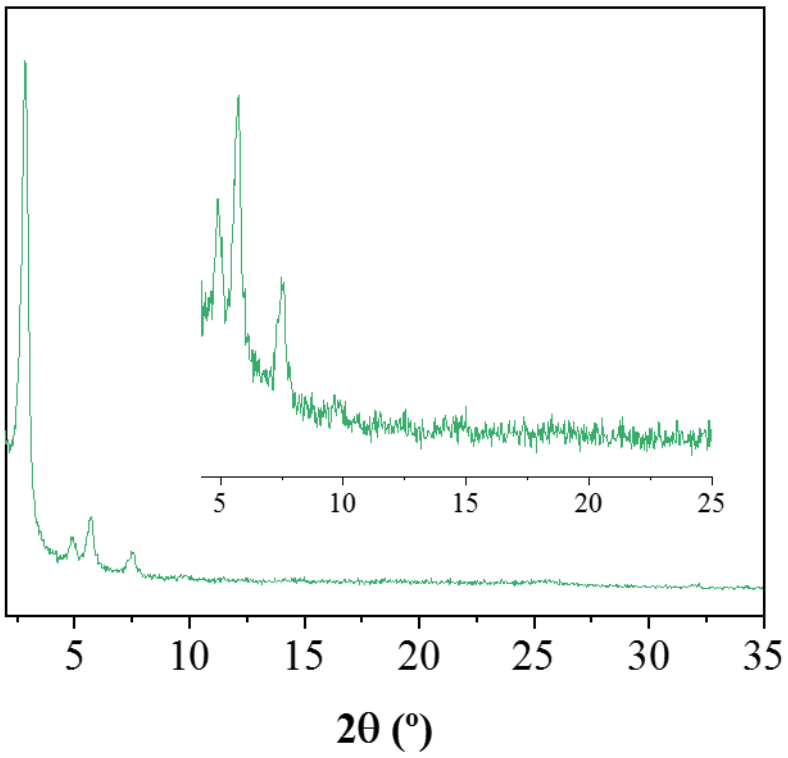

Figure S17. PXRD of PS3-COF and a magnification between 4º and 25º.

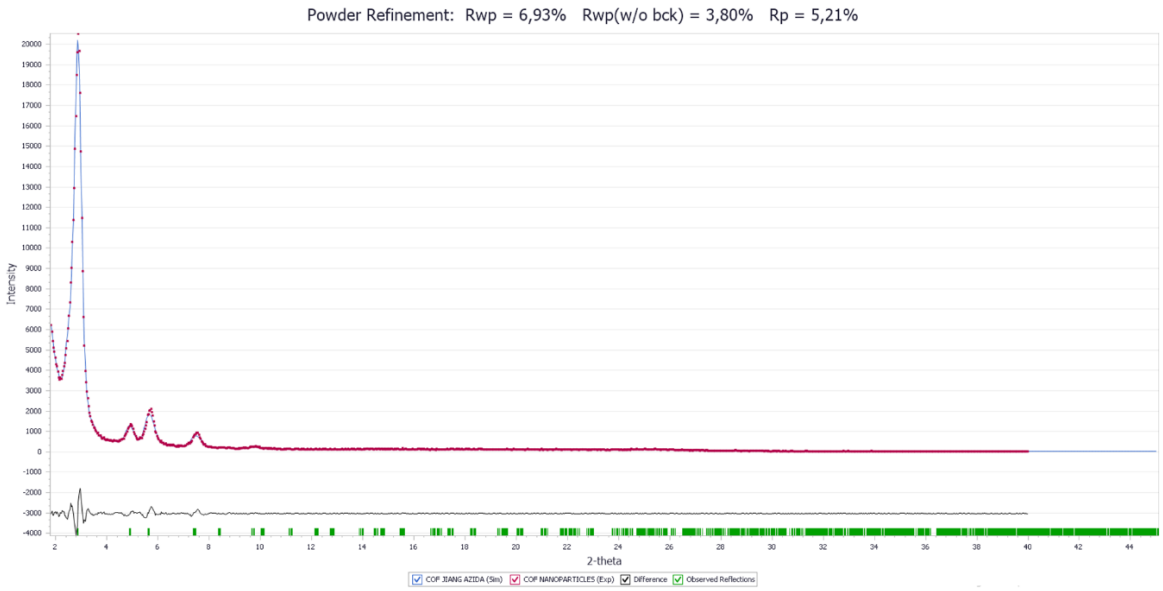

Figure S18. Results of Pawley refinement of COF nanoparticles.

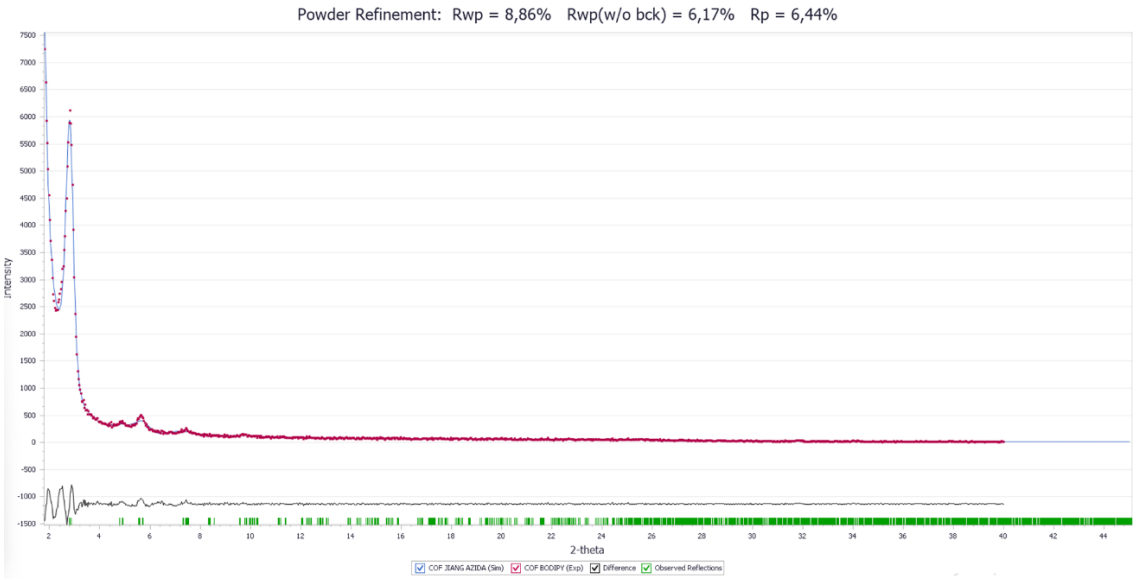

Figure S19. Results of Pawley refinement of PS1-COF.

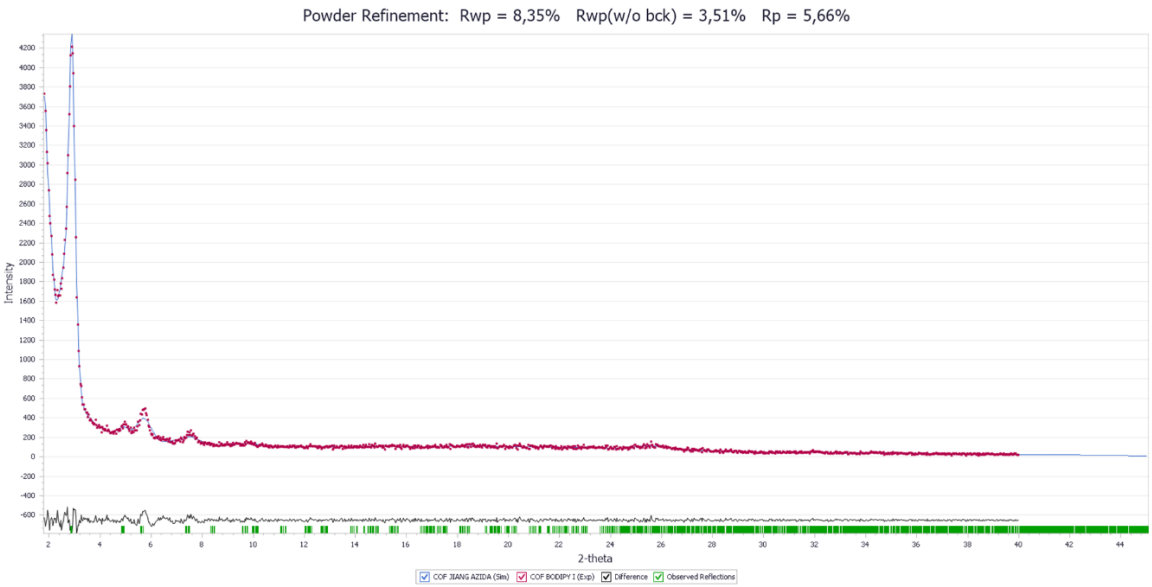

Figure S20. Results of Pawley refinement of PS2-COF.

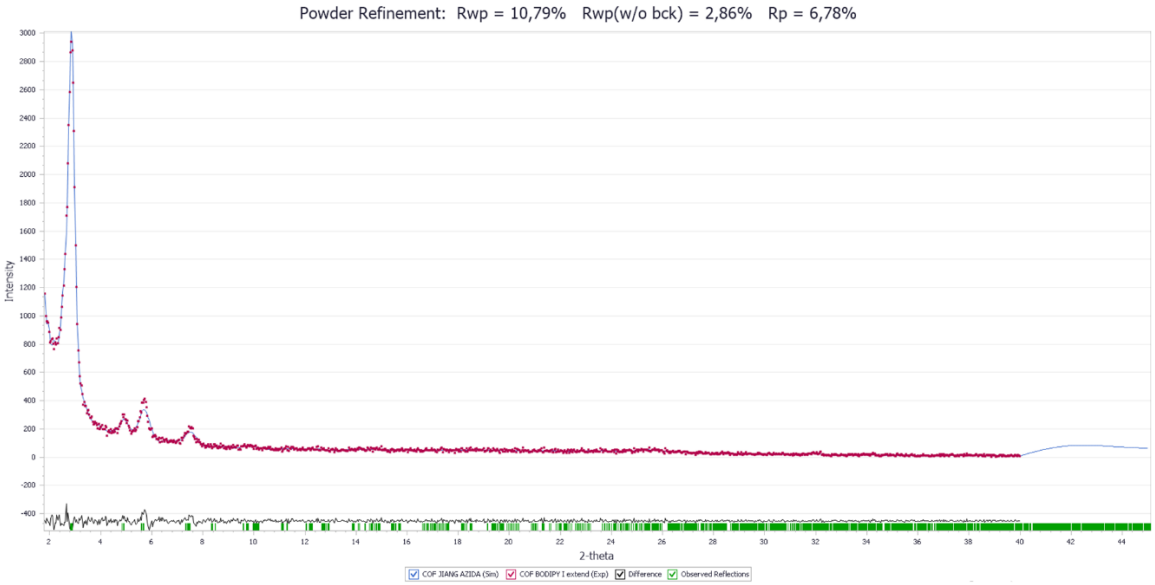

Figure S21. Results of Pawley refinement of PS3-COF.

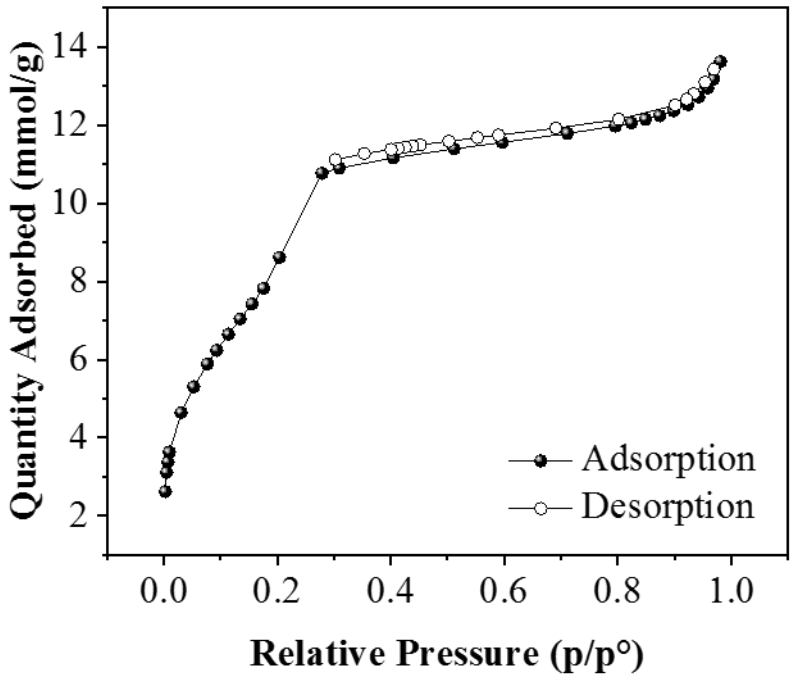

Figure S22. N_2 sorption isotherm for COF nanoparticles.

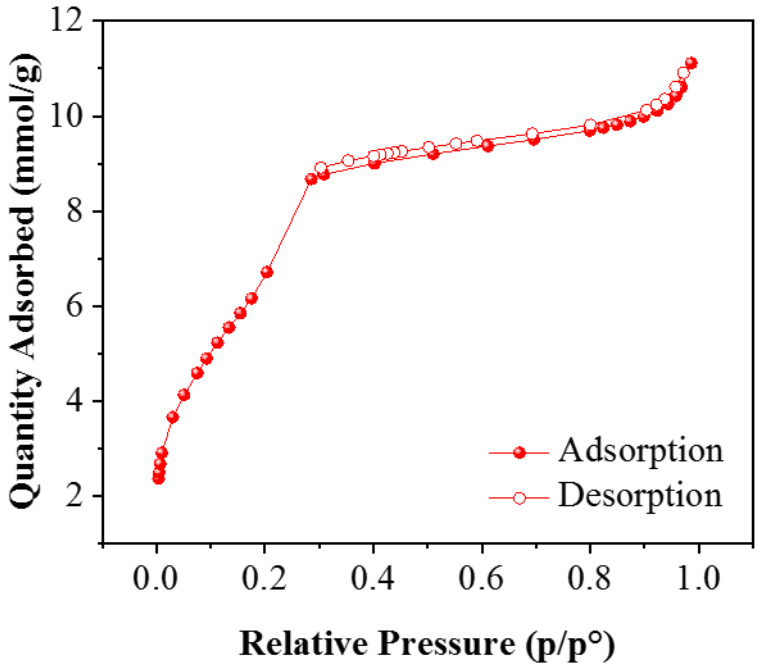

Figure S23. N_2 sorption isotherm for PS1-COF.

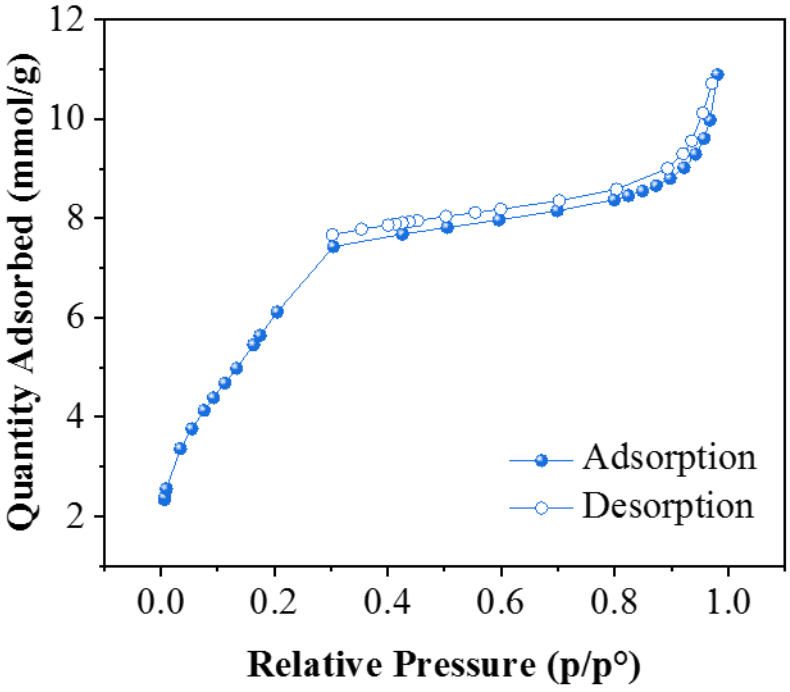

Figure S24. N_2 sorption isotherm for PS2-COF.

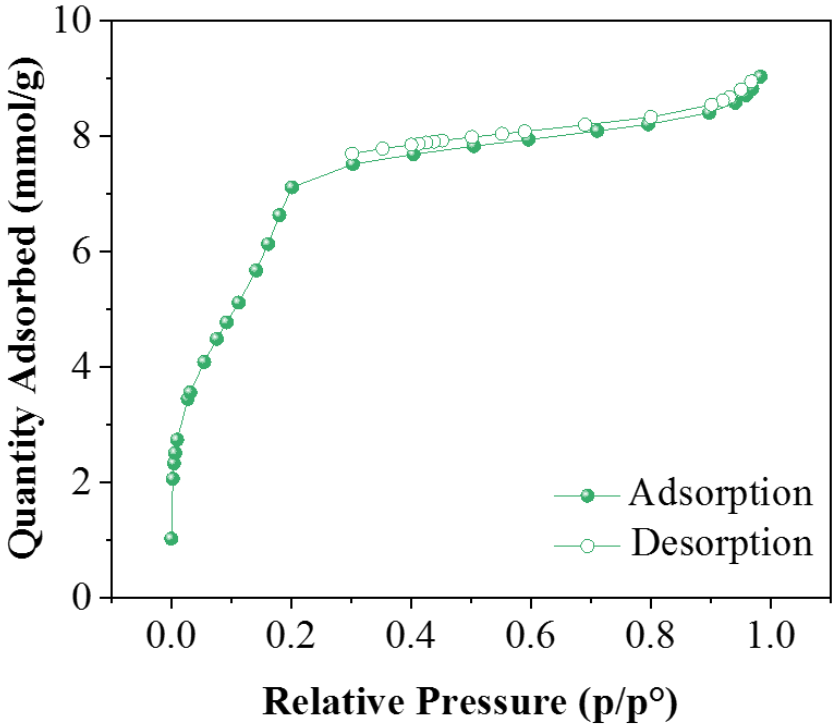

Figure S25. N_2 sorption isotherm for PS3-COF.

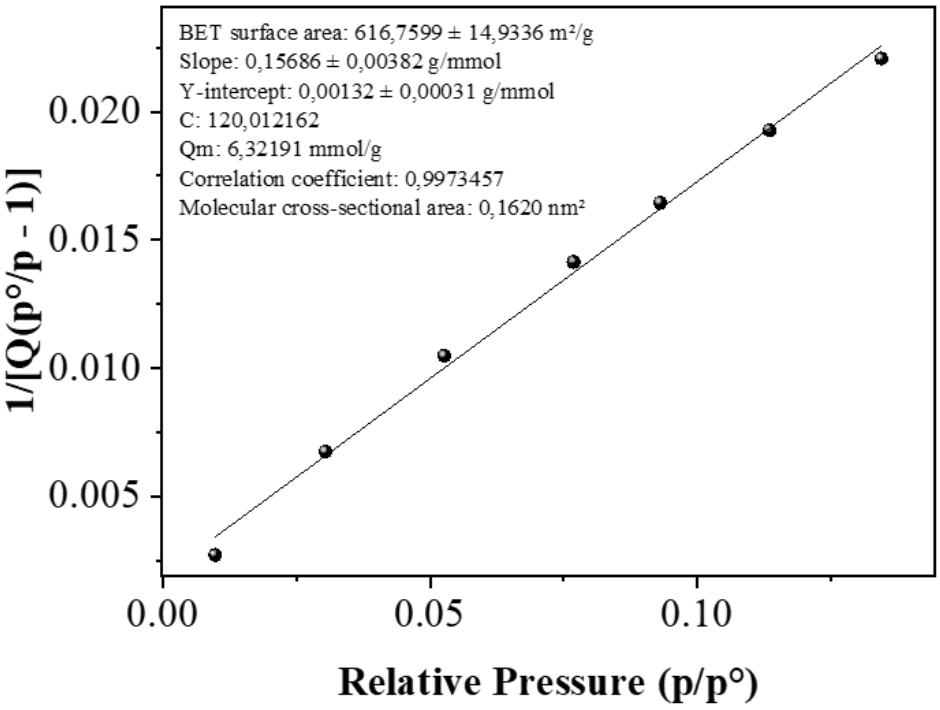

Figure S26. BET plot for nitrogen sorption of COF nanoparticles.

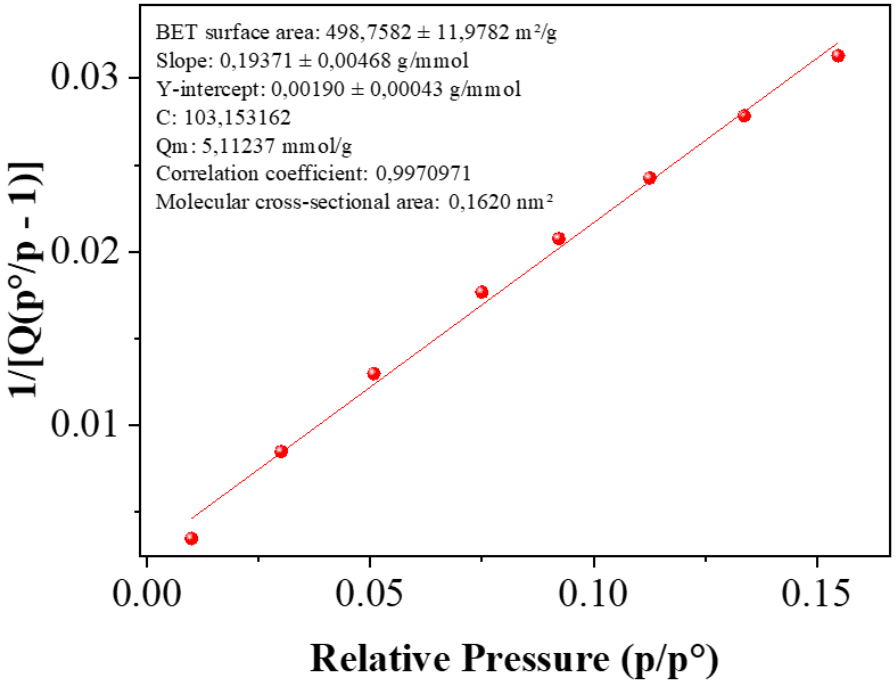

Figure S27. BET plot for nitrogen sorption of PS1-COF.

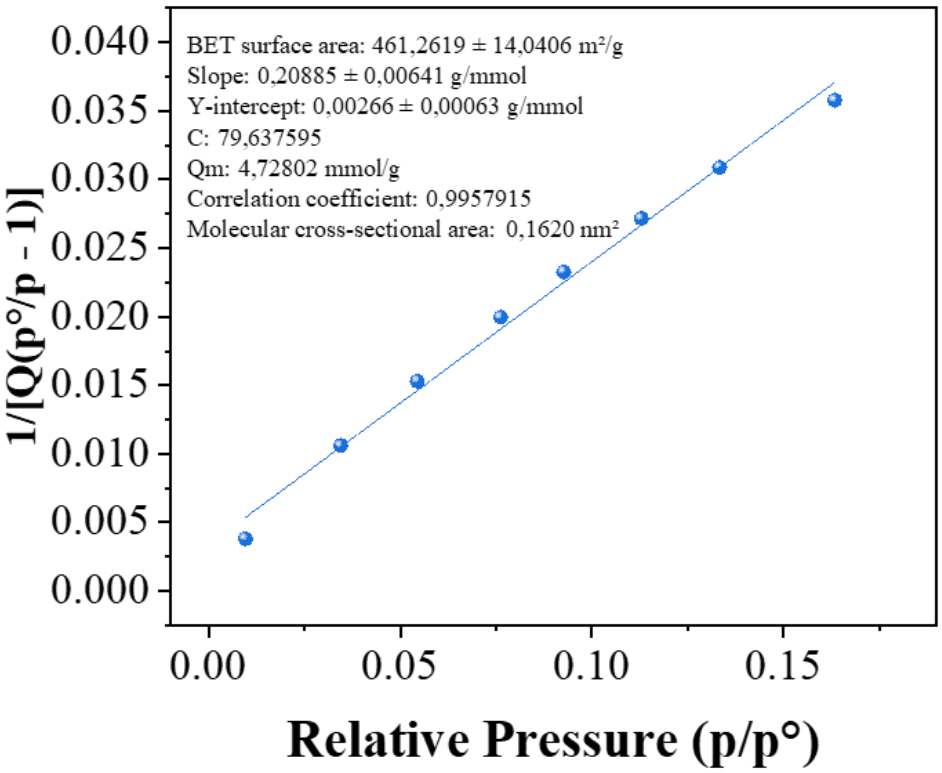

Figure S28. BET plot for nitrogen sorption of PS2-COF.

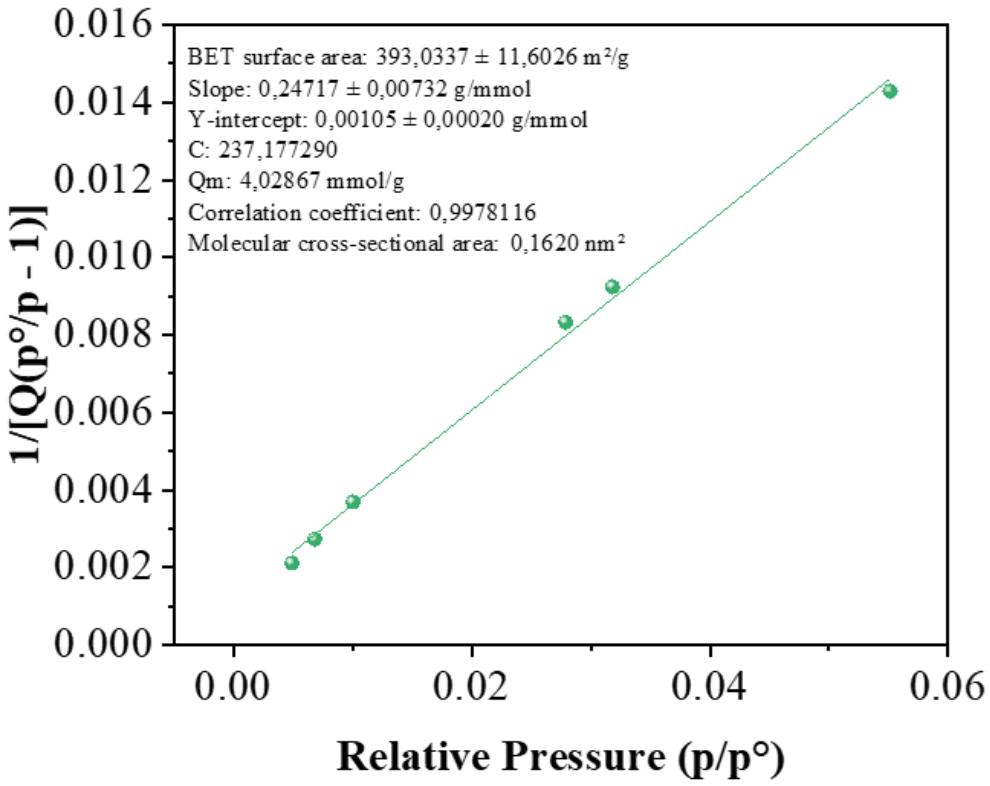

Figure S29. BET plot for nitrogen sorption of PS3-COF.

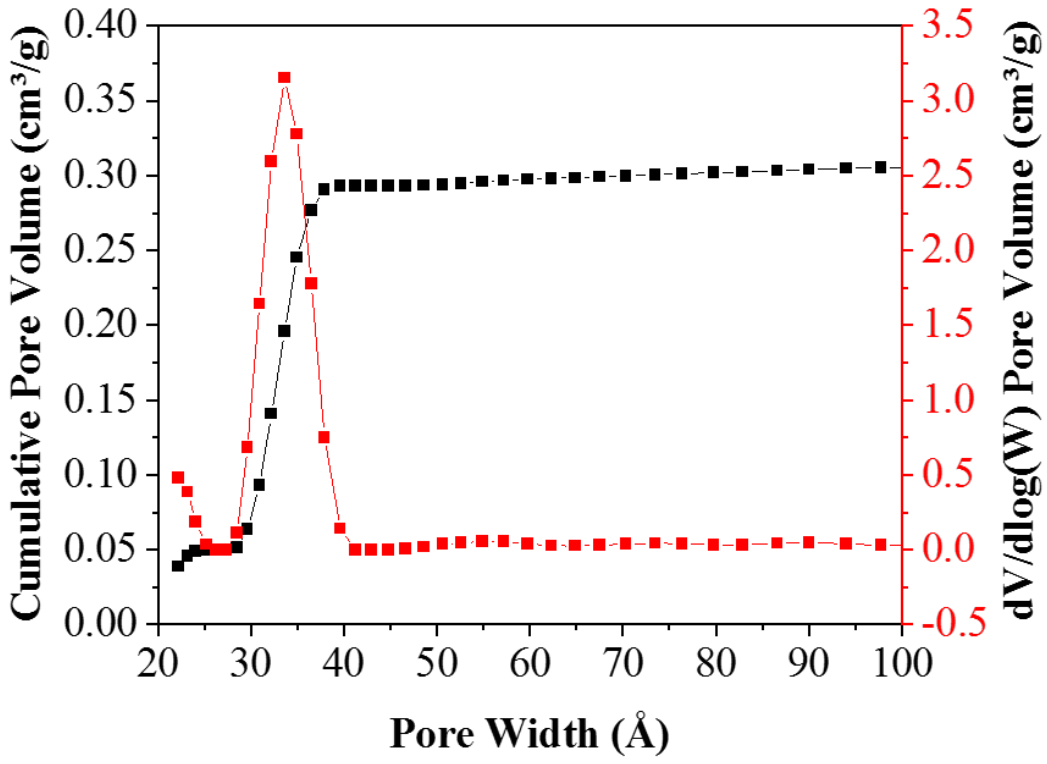

Figure S30. Cumulative pore volume and pore size distribution for COF nanoparticles.

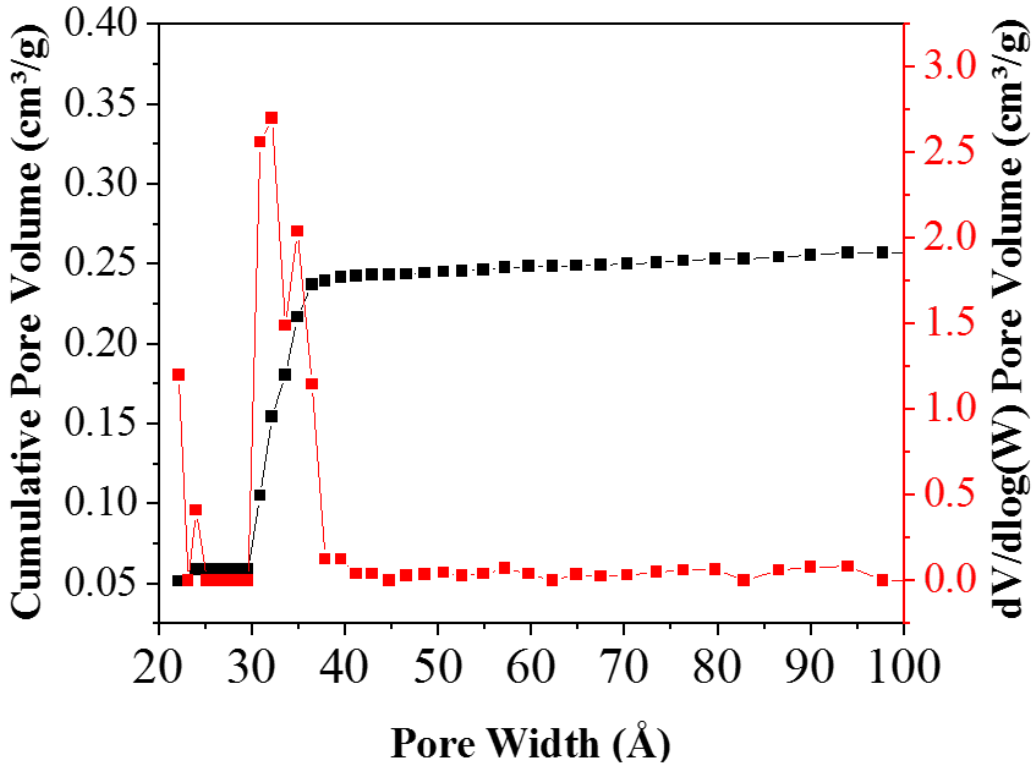

Figure S31. Cumulative pore volume and pore size distribution for PS1-COF.

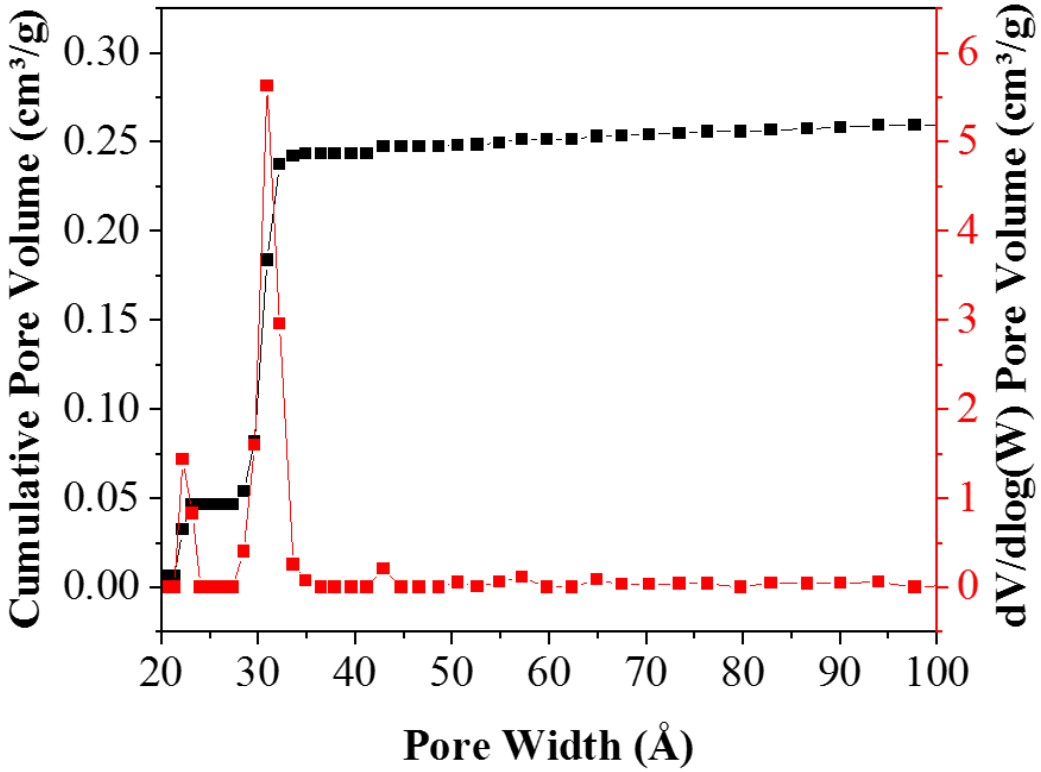

Figure S32. Cumulative pore volume and pore size distribution for PS2-COF.

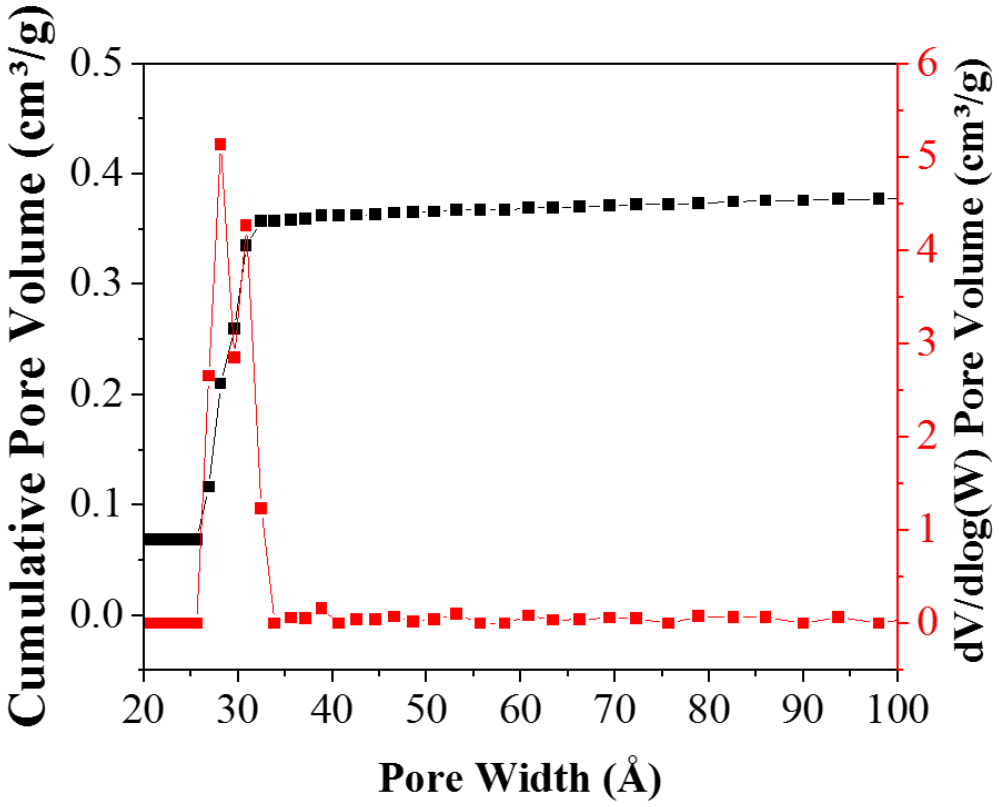

Figure S33. Cumulative pore volume and pore size distribution for PS3-COF.

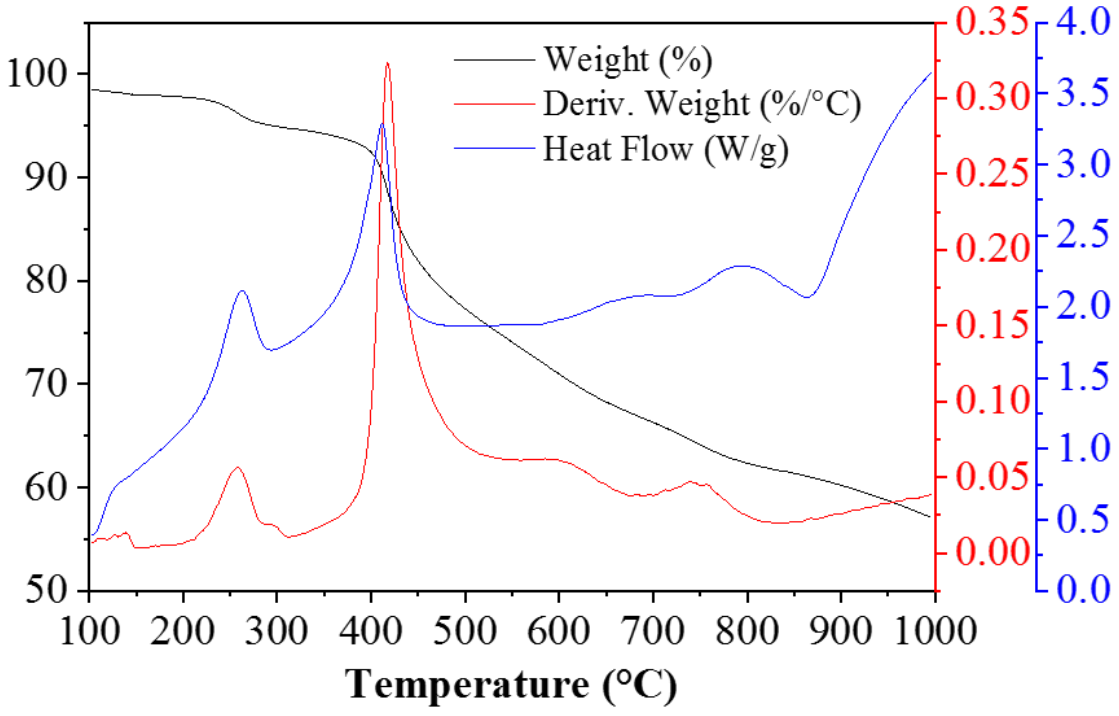

Figure S34. TGA and DSC analysis for COF nanoparticles.

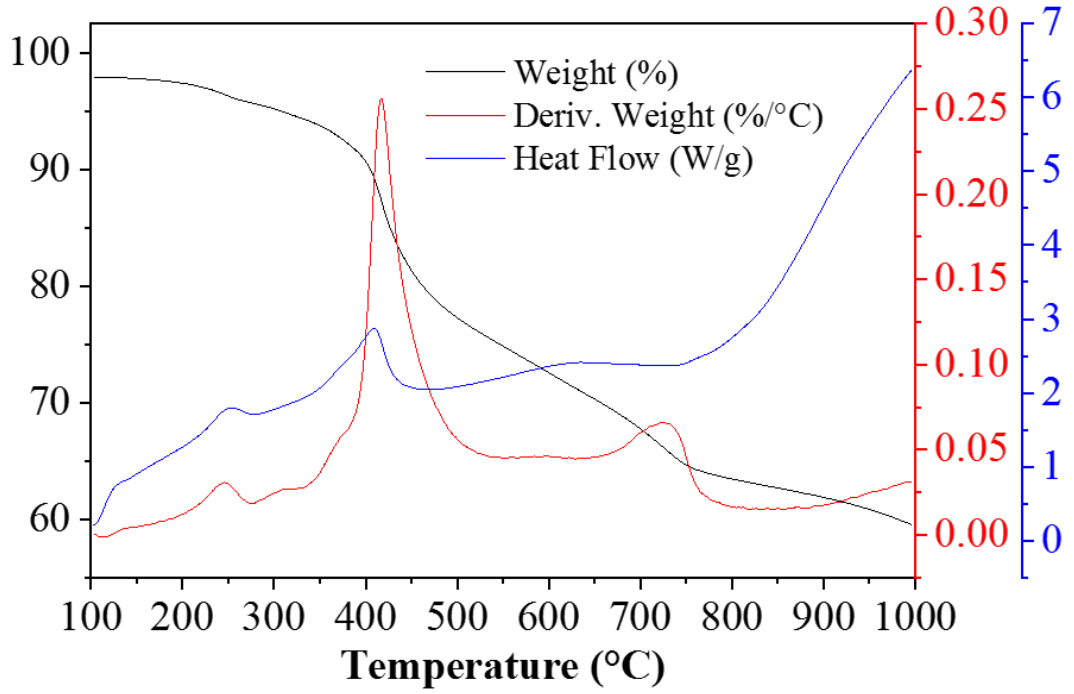

Figure S35.TGA and DSC analysis for PS1-COF.

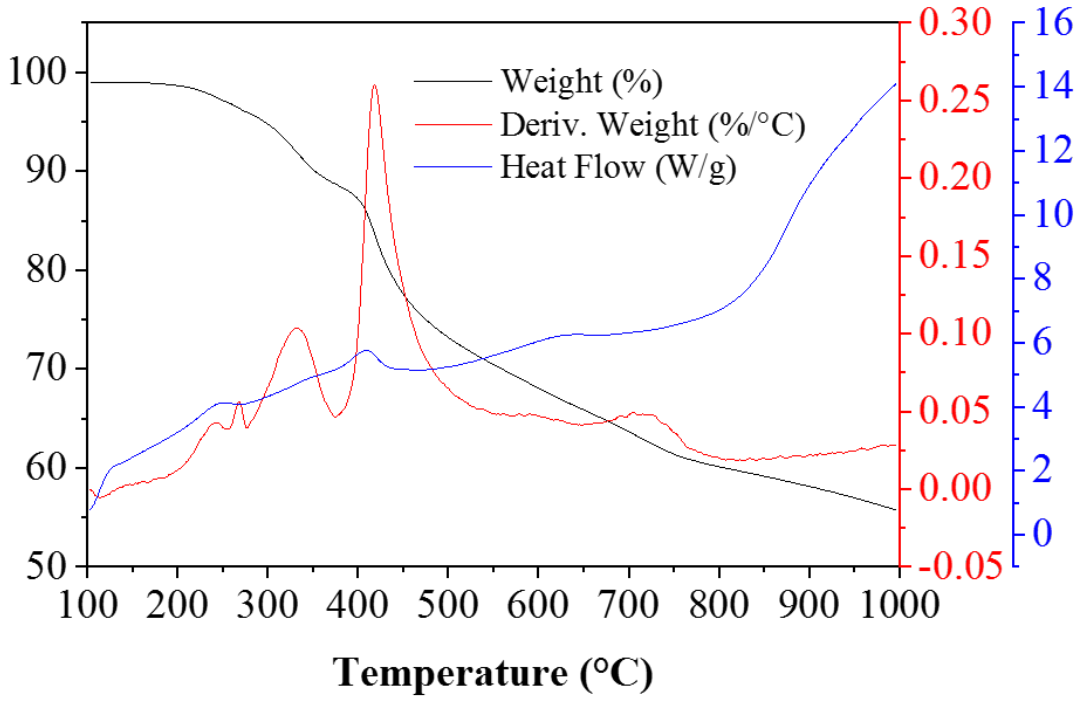

Figure S36. TGA and DSC analysis for PS2-COF.

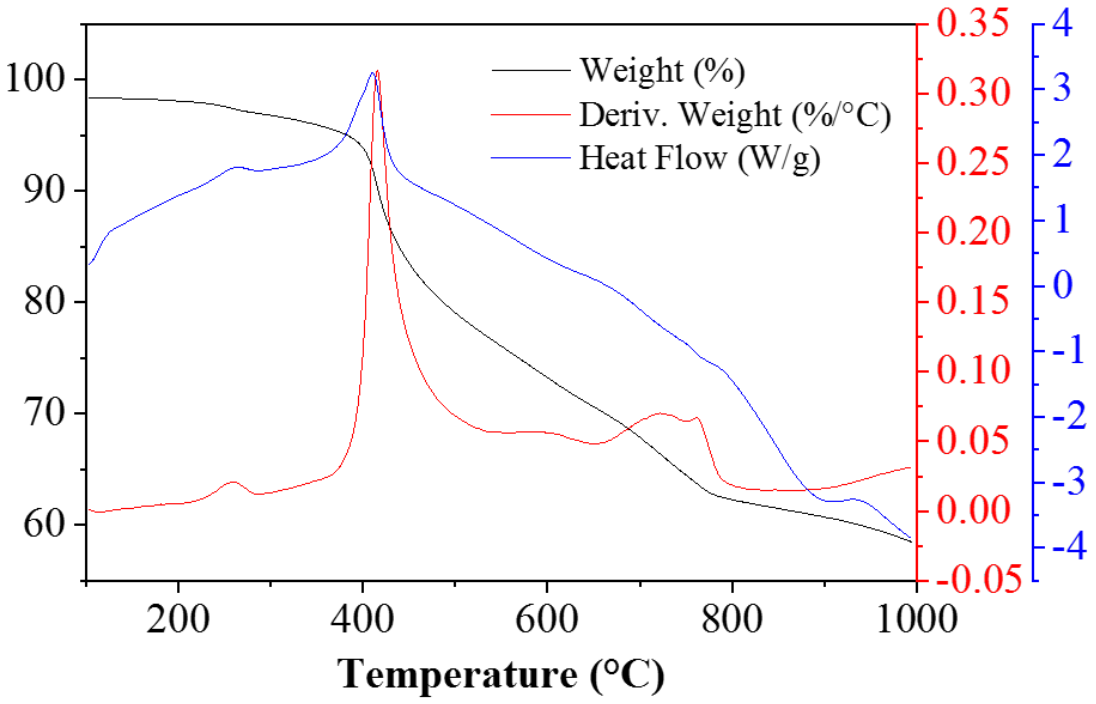

Figure S37. TGA and DSC analysis for PS3-COF.

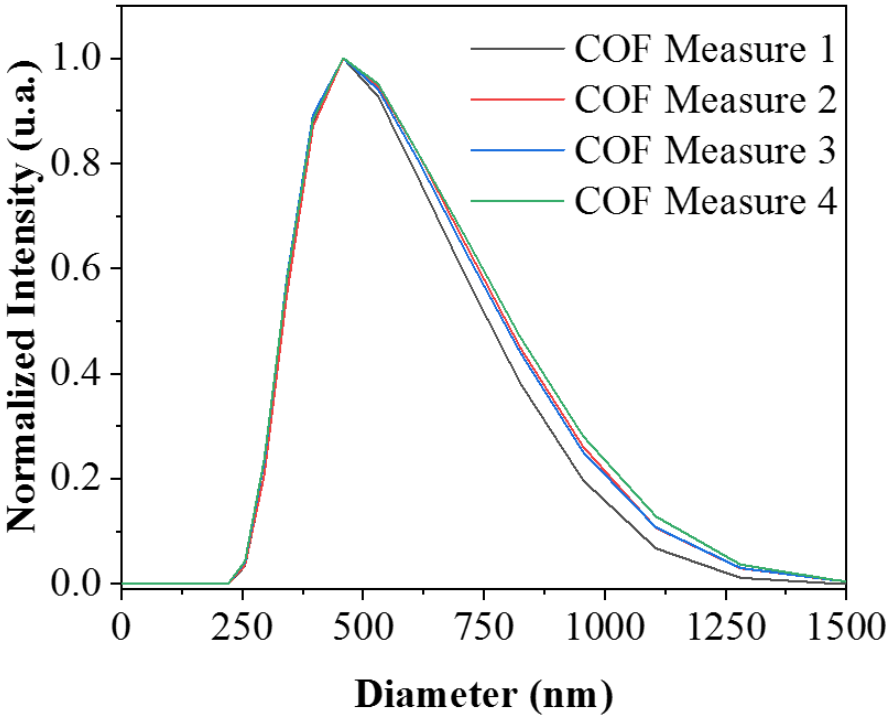

Figure S38. DLS measurements for COF nanoparticles.

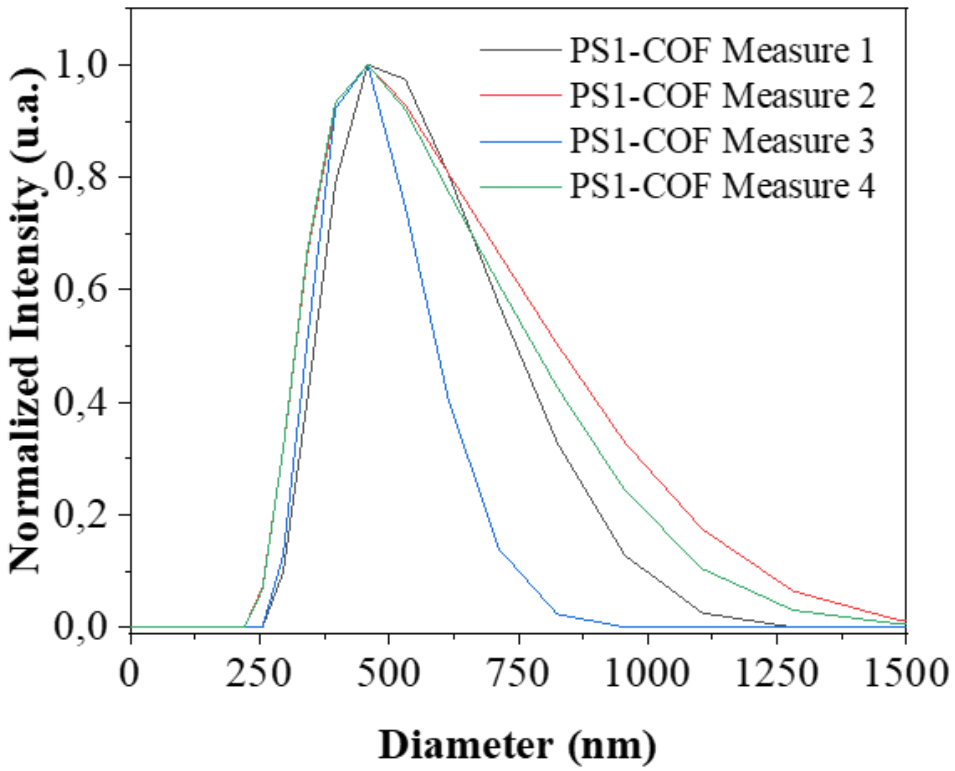

Figure S39. DLS measurements for PS1-COF.

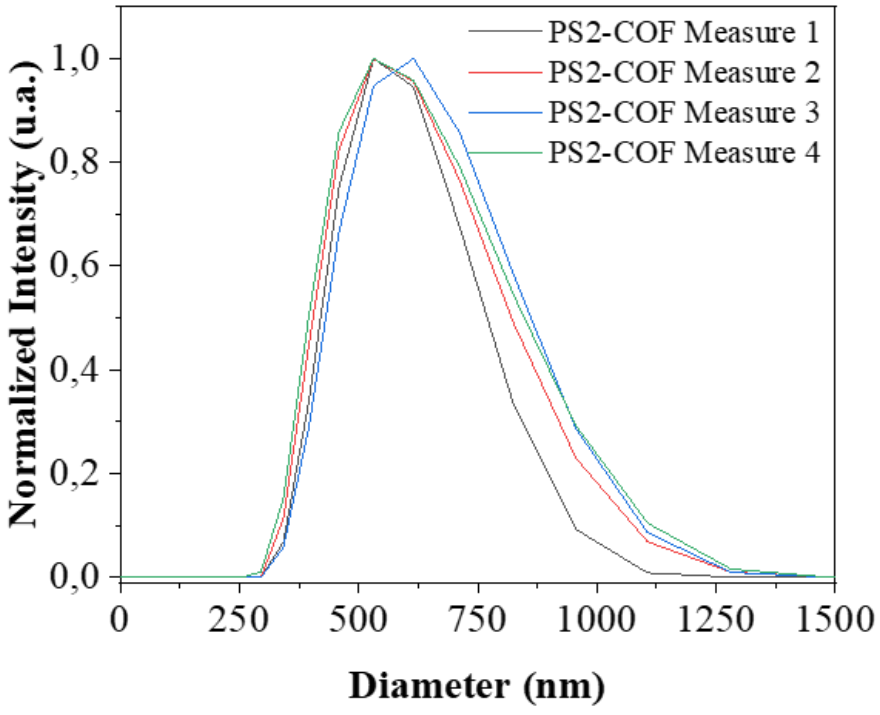

Figure S40. DLS measurements for PS2-COF.

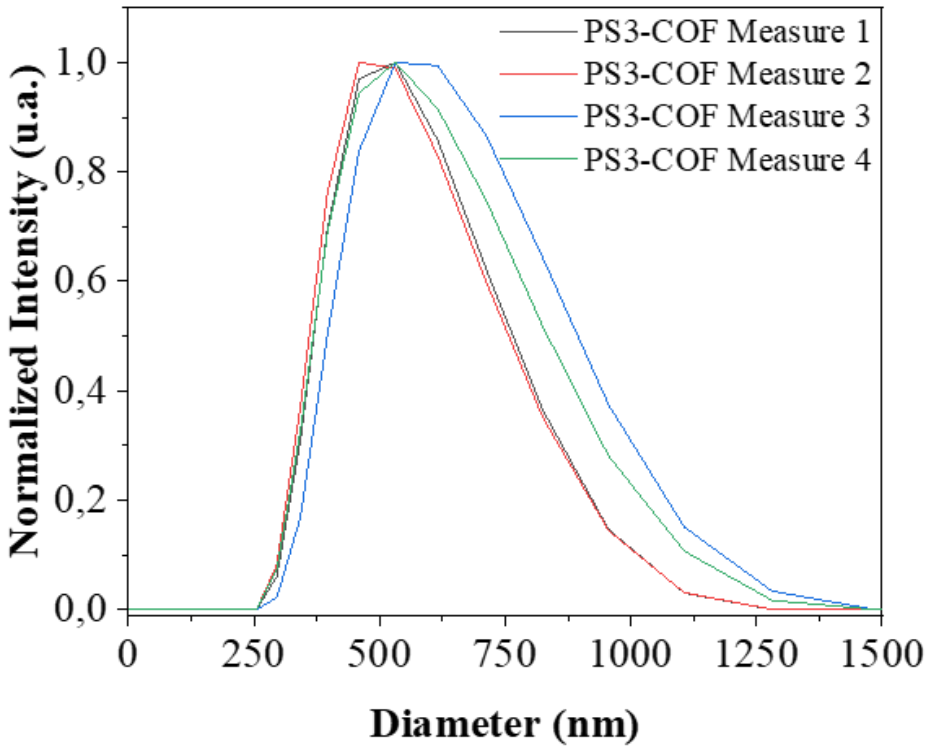

Figure S41. DLS measurements for PS3-COF.

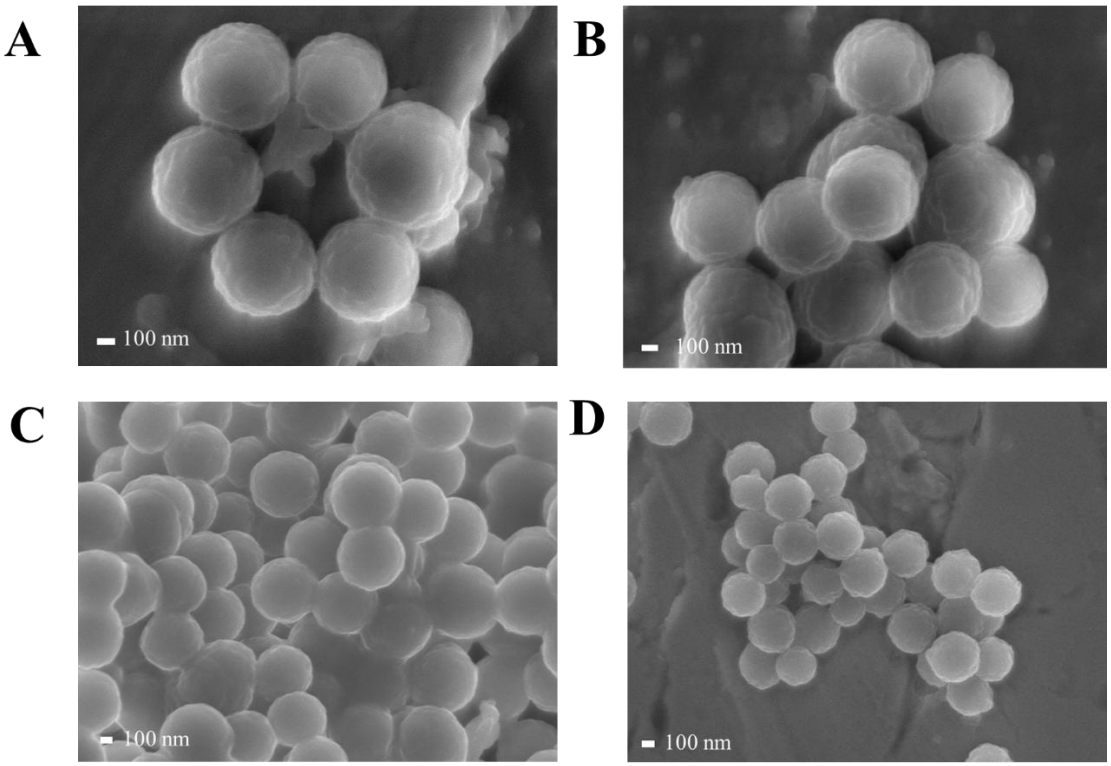

Figure S42. SEM micrographs of A) COF nanoparticles, B) PS1-COF, C) PS2-COF and D) PS3-COF.

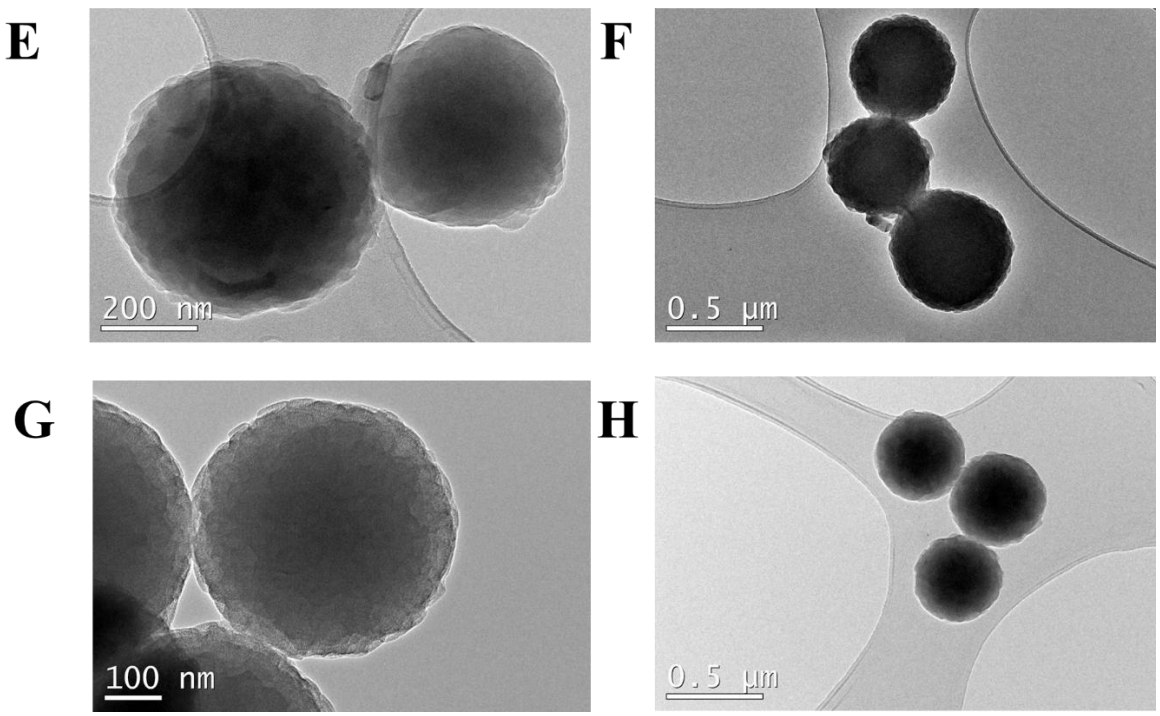

Figure S43. TEM micrographs of A) COF nanoparticles, B) PS1-COF, C) PS2-COF and D) PS3-COF.

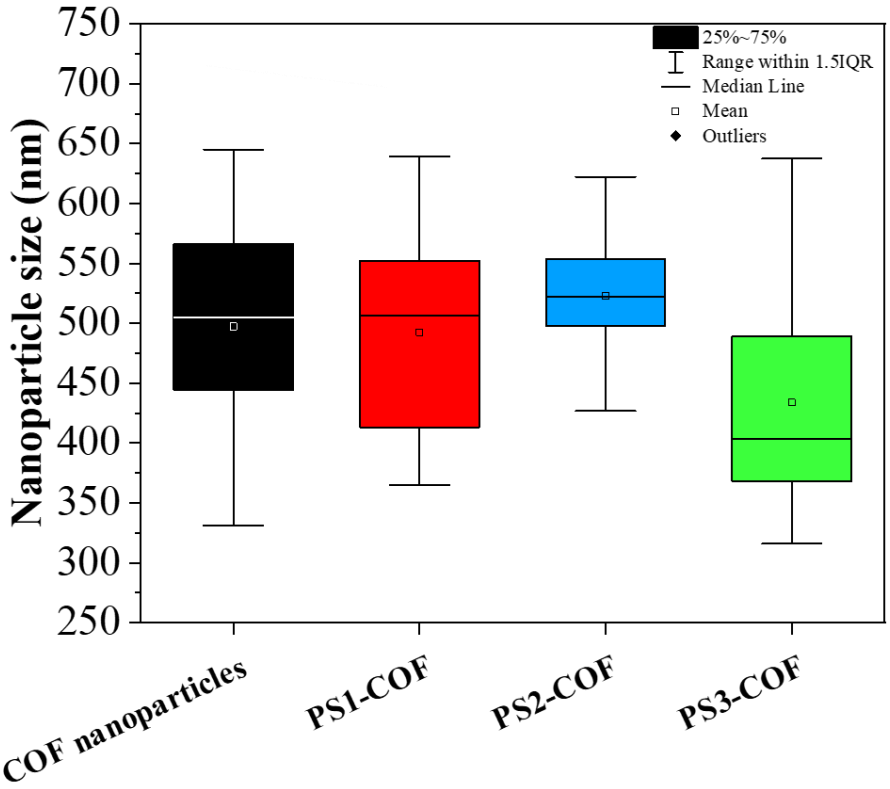

Figure S44. Statistical information for the measurements of the nanoparticle's sizes in SEM and TEM micrographs. (**Statistical analysis:** ANOVA analysis was performed with Origin 2021 software).

Section S3. Photophysical characterization

Table S1. Photophysical properties of **PS1-3** BODIPYs in diluted solutions (2 μM)

	λ_{ab} (nm)	ε_{max} (10^4 $M^{-1}\cdot cm^{-1}$)	λ_{fl} (nm)	ϕ_{fl}	τ_{fl} (ns)	ϕ^{Δ}
PS1						
c-hex	502.5	6.7	513.0	0.44	2.41	-
$CHCl_3$	503.0	6.0	513.0	0.47	3.43	0
MeCN	497.5	6.0	508.5	0.40	3.18	-
PS2						
c-hex	536.0	10.2	548.0	0.05	0.36	-
$CHCl_3$	536.0	9.7	552.0	0.04	0.31	0.91
MeCN	529.0	8.4	547.5	0.02	0.20	-
PS3*						
EtOAc	633.0	7.5	652.0	0.25	1.45(77%)-2.29(23%)	-
$CHCl_3$	641.0	8.0	660.0	0.27	1.59(84%)-2.49(16%)	0.74
MeCN	630.0	6.2	652.0	0.23	1.47(90%)-2.54(10%)	-

*not soluble in apolar media like c-hexane

Absorption (λ_{ab}) and fluorescence (λ_{fl}) wavelength, molar absorption at the maximum (ε_{max}), fluorescence quantum yield (ϕ_{fl}) and fluorescence lifetime (τ_{fl}),$^1O_2$ photo-generation quantum yield (ϕ^{Δ}).

c-hex: cyclohexane; EtOAc: ethyl acetate; $CHCl_3$: chloroform; MeCN: acetonitrile

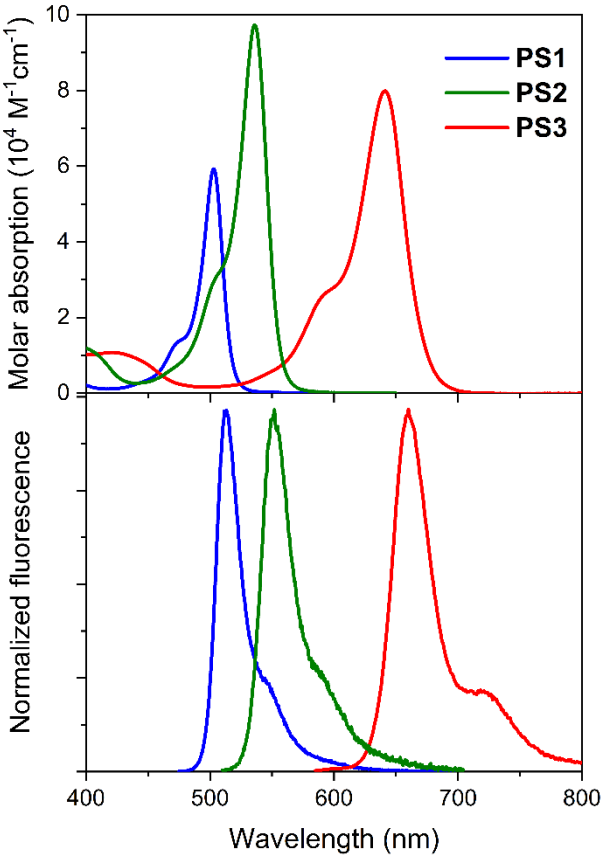

Figure S45. Absorption (up) and normalized fluorescence (bottom) spectta of PS1-3 BODIPYs in diluted solutions of chloroform (2 μM).

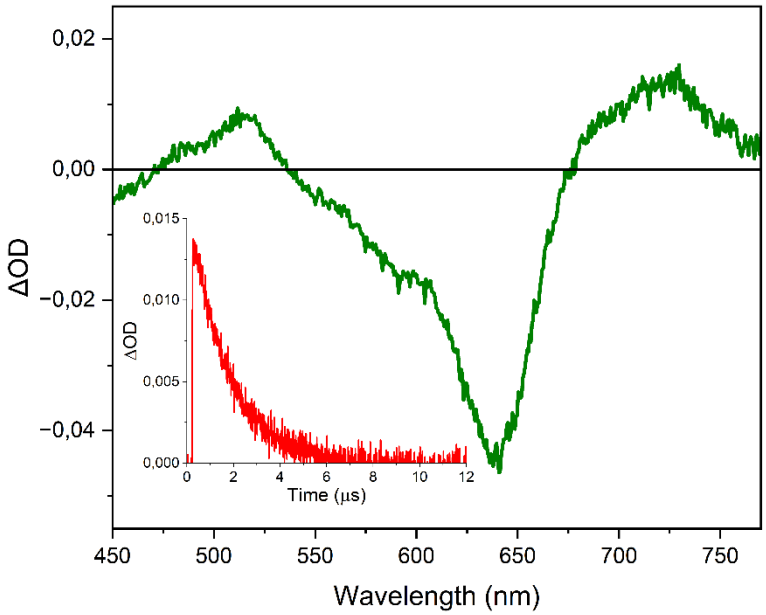

Figure S46. Nanosecond-transient absorption spectra and decay (inset) of PS3 BODIPY in chloroform under nitrogen saturated atmosphere.

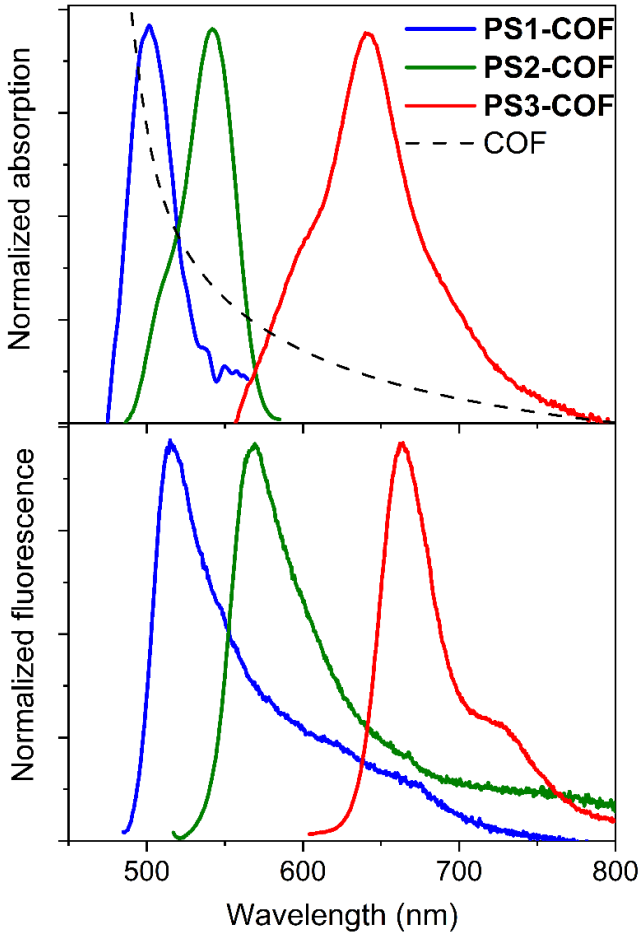

Figure S47. Normalized absorption (up) and fluorescence (bottom) spectta of PS1-, PS2- and PS3-COF suspensions in cloroform. The absorption spectrum of the COF itself without the dye (dashed line) is also included.

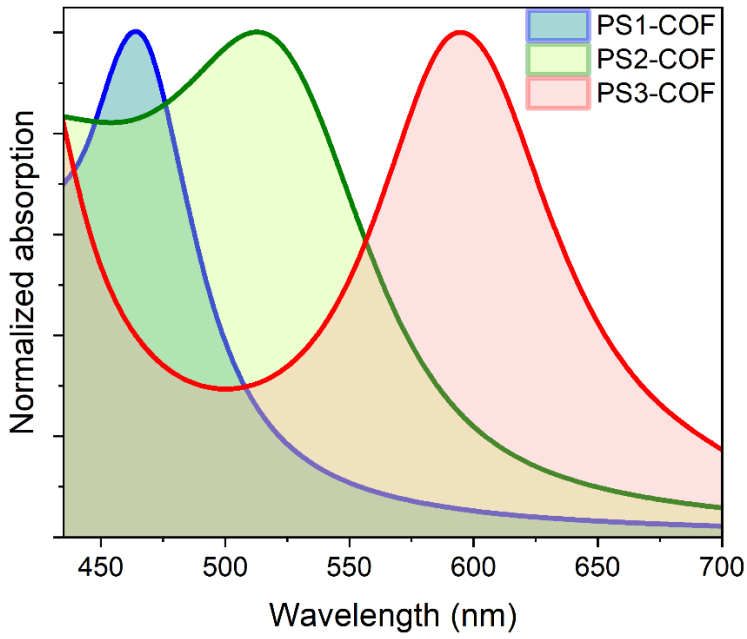

Figure S48. TDDFT photoabsorption spectra for the periodic models of PS1 (blue), PS2 (green), and PS3 (red) with two BODIPYs per pore.

Section S4. Biological studies

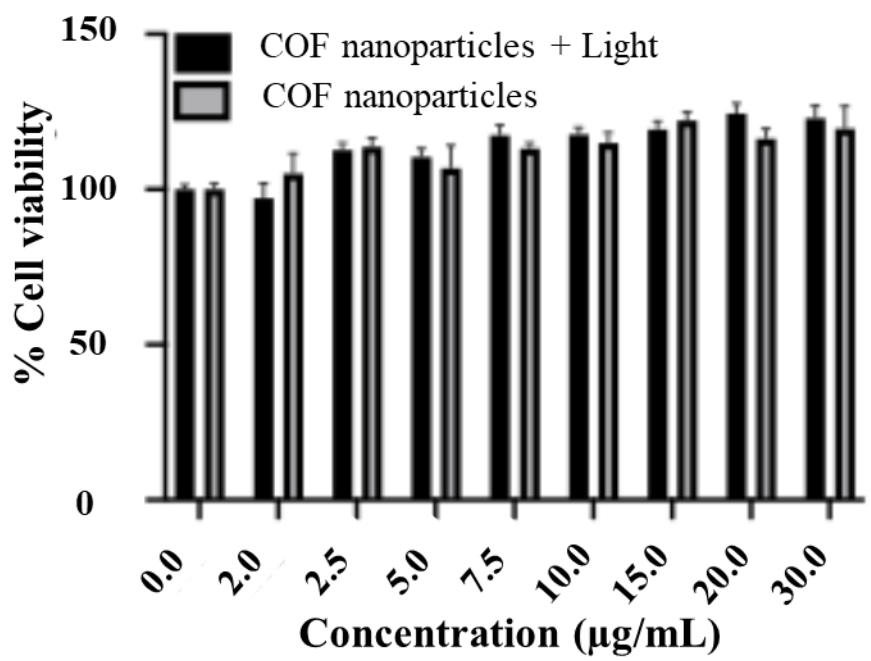

Figure S49. Photocytotoxic assay in SK-Mel-103 cancer cells of COF nanoparticles. Cells were treated with increasing concentrations within the range of 2 to 30 µg/mL for 24 h before irradiation for 30 min. Cell viability was determined 24 h after the irradiation step with WST-1 reagent. Values are expressed as mean ± SEM, and statistical significance was assessed by two-way ordinary ANOVA (n = 3).

Section S5. References

(1) Martínez-Fernández, M.; Martínez-Periñán, E.; Martínez, J. I.; Gordo-Lozano, M.; Zamora, F.; Segura, J. L.; Lorenzo, E. Evaluation of the Oxygen Reduction Reaction Electrocatalytic Activity of Postsynthetically Modified Covalent Organic Frameworks. *ACS Sustain Chem Eng* **2023**, *11* (5), 1763–1773. https://doi.org/10.1021/acssuschemeng.2c05826.

(2) Frisch, M. J. ea; Trucks, G. W.; Schlegel, H. B.; Scuseria, G. E.; Robb, M. A.; Cheeseman, J. R.; Scalmani, G.; Barone, V.; Petersson, G. A.; Nakatsuji, H. Gaussian 16, Revision C. 01. Gaussian, Inc., Wallingford CT 2016.

(3) Zhao, Y.; Truhlar, D. G. The M06 Suite of Density Functionals for Main Group Thermochemistry, Thermochemical Kinetics, Noncovalent Interactions, Excited States, and Transition Elements: Two New Functionals and Systematic Testing of Four M06-Class Functionals and 12 Other Functionals. *Theor Chem Acc* **2008**, *120* (1–3), 215–241. https://doi.org/10.1007/s00214-007-0310-x.

(4) Woon, D. E.; Dunning, T. H. Gaussian Basis Sets for Use in Correlated Molecular Calculations. III. The Atoms Aluminum through Argon. *J Chem Phys* **1993**, *98* (2), 1358–1371. https://doi.org/10.1063/1.464303.

(5) Clark, S. J.; Segall, M. D.; Pickard, C. J.; Hasnip, P. J.; Probert, M. I. J.; Refson, K.; Payne, M. C. First Principles Methods Using CASTEP. *Z Kristallogr Cryst Mater* **2005**, *220* (5–6), 567–570. https://doi.org/10.1524/zkri.220.5.567.65075.

(6) Perdew, J. P.; Burke, K.; Ernzerhof, M. Generalized Gradient Approximation Made Simple. *Phys Rev Lett* **1996**, *77* (18), 3865–3868. https://doi.org/10.1103/PhysRevLett.77.3865.

(7) Tkatchenko, A.; Scheffler, M. Accurate Molecular Van Der Waals Interactions from Ground-State Electron Density and Free-Atom Reference Data. *Phys Rev Lett* **2009**, *102* (7), 073005. https://doi.org/10.1103/PhysRevLett.102.073005.

(8) Vanderbilt, D. Soft Self-Consistent Pseudopotentials in a Generalized Eigenvalue Formalism. *Phys Rev B* **1990**, *41* (11), 7892–7895. https://doi.org/10.1103/PhysRevB.41.7892.

(9) Monkhorst, H. J.; Pack, J. D. Special Points for Brillouin-Zone Integrations. *Phys Rev B* **1976**, *13* (12), 5188–5192. https://doi.org/10.1103/PhysRevB.13.5188.

(10) Hirata, S.; Head-Gordon, M. Time-Dependent Density Functional Theory within the Tamm–Dancoff Approximation. *Chem Phys Lett* **1999**, *314* (3–4), 291–299. https://doi.org/10.1016/S0009-2614(99)01149-5.